Composite Structures 320 (2023) 117203

Contents lists available at ScienceDirect

Composite Structures

journal homepage: www.elsevier.com/locate/compstruct

Review

The opportunities and challenges of hybrid composite driveshafts and their couplings in the aerospace industry: A review

W. Jarrett [a,*], S.P. Jeffs [a], F. Korkees [b], M. Rawson [c]

[a] Institute of Structural Materials, Faculty of Science and Engineering, Bay Campus, Swansea University, Swansea SA1 8EN, UK
[b] Materials Research Centre, Faculty of Science and Engineering, Bay Campus, Swansea University, Swansea SA1 8EN, UK
[c] Rolls-Royce Plc, P.O. Box 31, Derby, DE24 8BJ, UK

ARTICLE INFO

Keywords:
Composite driveshafts
Hybrid driveshafts
Carbon fibre
Aerospace driveshafts
FRP driveshafts
Driveshaft corrosion

ABSTRACT

This article will analyse and discuss the ongoing research into the bonding of composite and metallic materials and their application in hybrid material driveshafts for the aerospace industry. The introduction of fibre reinforced polymers (FRPs) has been shown to dramatically decrease driveshaft weight, improve vibrational characteristics, and offer increased simplicity. However, the limited replacement of metallics with composites in the aerospace industry owes to the fact that there has been limited research into joining methods, failure modes and susceptibility to corrosion and temperature changes. This article covers a review of composite lay-up and coupling design, interface integrity, and the effect of corrosion and coefficient of thermal expansion (CTE) mismatch on driveshaft performance across a range of operation conditions.

1. Introduction

Composite driveshafts are a hybrid design, consisting of metallic end fittings and flanges, bridged by a fibre reinforced polymer (FRP), typically using carbon or glass (E-glass [1]) fibres. Specific to this design is the ability to keep weight down, with a typical carbon fibre reinforced polymer (CFRP) density two times and 5 times lower than aluminium and steel respectively [2]. This is all whilst maintaining the necessary torque carrying capabilities through the metallic ends. These weight savings can range from 10 % to 81 % compared with traditional metallic shafts [3,4,5,6,7]. Hybrid can also refer to differing reinforcements in a single composite layer; both uses of the term are employed in this article. With CFRP increasingly replacing traditional metallic driveshafts in aerospace, as well as studies suggesting they can be used for gas turbine engine components with active cooling [8] and without [9], it is vital to exploit these materials to their full potential and limits. There are studies for ultralight aircraft using CFRP/metallic hybrid driveshafts connecting piston engines with axial flow fans, where weight-saving is imperative [10], however, literature on composite/metallic hybrid driveshafts often focuses on the automotive industry, where the introduction of a composite to the metal eliminates the need for a two-piece driveshaft commonly needed due composite's higher specific elastic modulus [11]. A two-piece metallic driveshaft often involves three universal joints, a bearing, and a bracket, all of which are susceptible to damage from excess vibration and cause significant weight gain. Furthermore, an increase in length that a two-piece driveshaft inevitably gives, leads to a significantly lower whirling speed RPM, which is inversely proportional to shaft length [12].

This review article explores the opportunities and challenges of several key areas associated with the design and application of hybrid driveshafts including composite windings, coupling design, interfacial integrity and the influence of corrosion, moisture absorption and thermal expansion. Mechanical testing under torsion and analysing properties from torsional strength to natural frequency will be discussed. It will explore how the composite/metallic interfacial integrity varies under sub-zero and elevated temperatures, building on a review by **Zhao X et al** [13]. Table 1 provides an overview of the different source materials used in compiling this article, providing details of discipline, material, research purpose and major findings split across five categories: windings, couplings, interfacial integrity, corrosion and immersion and, coefficient of thermal expansion. All driveshaft studies involved full scale testing unless otherwise stated.

Whilst work on these hybrid composite/metallic driveshafts has increased in recent years, focus on combining hybrid driveshaft research

* Corresponding author.
E-mail addresses: w.i.jarrett@swansea.ac.uk (W. Jarrett), s.p.jeffs@swansea.ac.uk (S.P. Jeffs), F.A.Korkees@swansea.ac.uk (F. Korkees), Martin.Rawson@Rolls-Royce.com (M. Rawson).

https://doi.org/10.1016/j.compstruct.2023.117203
Received 29 November 2022; Received in revised form 3 May 2023; Accepted 29 May 2023
Available online 1 June 2023

Table 1
Details of sourced research material.

Source	Discipline	Material /Geometry	Purpose	Major findings
Driveshaft Design: Windings				
Poul R et al [10]	Aerospace	*Material:* Aluminium/CFRP hybrid *Geometry:* Hollow shaft, aluminium flanges *Winding pattern:* HSC [±45/0/±45] HSC, HMC, HSC [±34/0/±85]	Compare traditional aluminium and aluminium/CFRP hybrid driveshafts and assess the effect of the integrating high-modulus carbon (HMC) on torsional properties.	Aluminium shaft: Showed a medium longitudinal stiffness, highest torsional stiffness, and weight, all disadvantageous. Hybrid shaft without HMC showed a relatively low axial stiffness and of too high torsional stiffness. Hybrid shaft with integrated HMC: considered the best design.
Nayak et al [5]	Automotive	*Material:* CFRP *Geometry:* Hollow shaft, aluminium flanges *Winding pattern:* $[85_2/\pm45_2/25_2]_S$	To assess the effect that replacing an all-steel driveshaft with a CFRP/aluminium flange shaft would have on torsional strength.	The CFRP shafts showed an 8.5% increase in average torsional strength whilst weighing 60% less. SEM imaging suggested that resin rich areas and outer-surface cracking led to a lower torsional strength.
Tariq M et al [14]	Aerospace / Automotive	*Material:* CFRP *Geometry:* Hollow shaft *Winding pattern:* $[0/\pm45]_n$	To discover how outer winding layer orientation and number of layers in total effects torsional properties.	Helix and hoop winding layer addition led to an increase and decrease in torsional strength, respectively. An increase in layers lead to a decrease in maximum angle of twist. Torsional stiffness increased with number of layers, regardless of type. Helix layer offered greater stiffness addition than hoop.
Sun Z et al [15]	Aerospace / Automotive	*Material:* CFRP *Geometry:* Hollow shaft, metallic flanges *Winding pattern:* $[(15–65)_{(1-6)}/90_2]$	To assess how ply angle and thickness affects natural frequency and damping, whilst comparing how the addition of metallic flanges to CFRP and whether the flange is glued or embedded affects these also.	Natural frequency decreased on average 63% and damping increased with an increase in ply angle from 15° to 65°. The addition of metallic and embedded flanges reduced the natural frequency over this range. Natural frequency decreased by 21% and damping also decreased over a ply decrease of 4.2 mm to 1.2 mm. The addition of metallic flanges reduced the natural frequency by 34%.
Prasad AS et al [16]	Automotive	*Material:* E-glass/Epoxy composite *Geometry:* Hollow shaft, metallic flanges *Winding pattern:* $[15/\pm54.7/\pm75/90]_S$	Optimal stacking sequence to meet static torque and bending natural frequency design specifications.	The torque bearing capability of the E-glass composite shaft out-performed the steel shaft by 75%. It was also found to withstand 10.5% greater buckling torque, 25.7 % higher stiffness and 25 % higher natural frequency.
Sevkat et al [17]	Automotive	*Material:* E-glass/carbon combined reinforcement composite *Geometry:* Hollow shaft, metallic flanges, hybrid reinforcements in separate layers *Winding pattern:* [-45/+45]	To investigate the effect that torsional strain-rate and lay-up sequence on torsional behaviour.	The results suggested that if carbon was used in layers with high shear stress, a higher torque could be achieved. Using glass in the outer layers offered a higher maximum twist and therefore ductility. A higher loading rate showed a decrease in twisting angle but with maximum torque staying largely the same, it concludes that very high torsional speeds of $5^\circ \cdot sec^{-1}$ do not jeopardise torsional strength.
Tariq et al [3]	Aerospace / Automotive	*Material:*(E-glass-carbon, aramid-carbon) composite *Geometry:* Hollow shaft, metallic flanges, hybrid reinforcements in same layer *Winding pattern:* $[90/\pm45]_n$	To investigate the torsional performance, chemical reactivity, hardness, and density and compare to a pure carbon fibre counterpart.	The addition of glass and aramid fibres decreased torsional properties by 43% and 23% respectively. No degradation of the shafts was found after saline submersion, but carbon-aramid shafts showed 21% weight loss after acidic immersion. Hardness increased 40 HV with the both reinforcement additions over carbon-only. The carbon-aramid shaft showed the greatest weight saving at 10%.
Driveshaft Design: Couplings				
Laberge et al [18,19]	Aerospace	*Material:* CFRP and steel *Geometry:* Sinusoidal composite webbing in bull gear.	To determine the performance of hybrid gearing with respect to torque, temperature and vibration. [19] also studied stepped composite thickness change over radius.	Maximum torque response: up to 27100 N·m, reducing weight by 4.5 kg. Vibration saw little change across both designs, aside from small variations at specific powers. No change to overall thermal behaviour of the gearbox initially, but for [19], the temperature difference between fling off and oil inlet was 2 °C to 5 °C higher. Measurements taken between lobes showed 50% more strain, decreasing with increasing composite step number from the inner radius.
Gauntt et al [20] and **Waller et al** [21]	Aerospace	*Material:*CFRP (BMI or Epoxy) and steel *Geometry:*	Composite layup sequence effect on vibration properties of the hybrid gear [20]. Effect of resin type (BMI vs Epoxy) on composite's 'oil-off' performance and compression strength [21].	Natural frequencies similar across all composite types, but up to 23.5% below the steel gear for some modes. Weight loss over the all-steel gear: 14.7% to 18.4% [20]. Over 204 °C, BMI resin offered the highest compression. Pitch-based

(*continued on next page*)

Table 1 (*continued*)

Source	Discipline	Material /Geometry	Purpose	Major findings
		Sinusoidal composite webbing in bull gear.		laminates retained a thermal conductivity similar to that of the steel comparison: (50 to 60) W·(m·K)$^{-1}$, but had a lower compression strength. Combining both fibre types led to a balance of both properties [21].
Kim et al [22]	Aerospace / Automotive	*Material:* CFRP and steel *Geometry:* Scarf joints, Single and double lap joints: Circular Hexagonal Elliptical	Tested the torque transmission capabilities of the following geometries: circular and circular with scarf single lap, circular and circular with scarf double lap, hexagonal and elliptical single lap.	Hexagonal single lap joints had maximum torque capability. Both the hexagonal and elliptical joints had higher capabilities over circular, the circular double lap joints had higher torque capabilities than single lap. The scarf joints showed no improvement in torque capabilities.
Lee et al [23]	Automotive	*Material:* CFRP/aluminium/ Steel *Geometry:* Hollow shaft with splines on outer diameter at either end, connecting to steel flanges *Testing scale:* reduced	Looked at the feasibility of designing a drive shaft where the flanges were designed with splines to increase their torque capabilities.	A Slip amplitude of 10 μm could be achieved with a spline aspect ratio of 0.25. The average shear strength of the spline joint was 34 MPa, 1.5 times higher than of a similar adhesively bonded joint without splines. Finally, neither delamination nor spline failure was found before buckling when torque testing.
Choi et al [24]	Aerospace / Automotive	*Material:* CFRP and steel *Geometry:* Single lap joints: Circular Triangular Tetragonal Pentagonal Hexagonal Elliptical	To study the effect that adhesive thickness, interfacial geometry and stacking sequence have on their torque transmission capabilities.	The static torque transmission capability of the adhesively bonded circular single lap joint increased as the adhesive thickness decreased. The adhesively bonded circular single lap joint had the largest static torque transmission capability when the stacking sequence of the composite material was $\pm 25^{\circ}$. There was a decrease in torque capability for triangular and tetragonal with an increase in angle, whilst pentagonal and hexagonal showed no clear correlation over the angle change. For elliptical, maximum torque capability was found at $\pm 30^{\circ}$.
Henry et al [25,26]	Aerospace/ Military	*Material:* [25]: CFRP [26]: CFRP/Steel *Geometry:* Composite tubes with interior collar steel flanges [26]	[25]: Multi-objective optimal design for composite rotorcraft driveshafts and [26]: to find a composite driveshaft design intended to reduce hanger bearings and increase survivability against armour piercing rounds.	[25]: A reduction in bearing and lamina number in the mid-span region had a negative impact on the whirling and buckling safety factors respectively. Lower fibre angles led to fibre-direction compressive stress. The matrix with the highest modulus of elasticity gave rise to the lightest designs. [26]: Higher damage influence on residual torsional stiffness for driveshafts with higher outer winding angles.
Interfacial Integrity				
Kim et al [27]	Automotive	*Material:* Carbon/glass fibre composite/aluminium *Geometry:* Hollow shaft with aluminium inserts adhesively bonded *Testing scale:* reduced	To assess how adhesive bonding length and insert thickness alters torque transmission capability of a driveshaft.	The torque transmission capabilities after 15 mm bonding length saturated in general, with 15 mm giving 4850 N·m. A 3 mm insert thickness led to the highest capabilities of 4840 N·m.
Alves et al [28]	Aerospace/ Automotive	*Material:* CFRP and aluminium *Geometry*:Scarf joint (plates)	To determine the effectiveness of dis-similar adherends in scarf joints, as well as the scarf angle effects on the joint's mechanical properties.	Stress variation along the width of the bond varied very little, and peaks were much reduced. There was shear stress asymmetry at either bond edge due to a variation in adherend stiffness. Ultimate joint strength occurred at 10°, but still reduced compared to aluminium only.
Carbas et al [29]	Aerospace	*Material:* Metal laminate modified CFRP *Geometry*:Single-lap (plates)	To assess the effect of adding aluminium sheets during composite manufacture to enhance the through-thickness mechanical properties, creating a fibre metal laminate.	Tensile testing showed that the addition of aluminium plating reduced instances of delamination leading to failure, and instead more cohesive failure. The ultimate hybrid lay-up was found when the aluminium layers were external, giving rise to the highest joint strength.
Jimenez-Vicaria J et al [30]	Civil	*Material:* CFRP and steel *Geometry*:Double-strap joint (plates)	To assess how CFRP stiffness and adhesive ductility had on bonding with steel and subsequent failure load.	For longer bond lengths of 60 mm, a ductile adhesive and stiff fibre gave more desirable results. For shorter bond lengths of 30 mm, the inverse was found. For example, there was found to be 49% higher failure load with a ductile adhesive compared to brittle.
Amraei et al [31]	Civil	*Material:* CFRP and steel *Geometry:*[25]Single and Double-sided join (Plates)	To assess how high and ultra-high strength steels compare to mild steel when bonded with CFRP.	When comparing to S700 mild steel, 960 HSS increased maximum bond load by 29.4–29.6%, and 1100 UHSS by 29.8–30.3%. Furthermore, single and double CFRP sided specimens reduced stress in the steel by 18% to 24% and 43% to 45% respectively.

(*continued on next page*)

Table 1 (*continued*)

Source	Discipline	Material /Geometry	Purpose	Major findings
Al-Mosawe et al [32]	Civil	*Material:* CFRP laminate and steel *Geometry:*Double-strap joint (plates)	To assess how loading rates affect the bond between CFRP and steel and subsequent joint capacity and failure mode.	There was found to be no link between differing loading rates and local bond stresses. There was, however, a strong link when comparing static vs dynamic loading in general. For example, a joint capacity increase of 50% for dynamic loading with a lower effective bond length. Failure was consistently found to be in the adhesive layer, suggesting it made the largest contribution to load bearing.
Al-Shawaf et al. (2006) [33]**and Al-Shawaf et al. (2013)** [34]	Civil	*Material:* CFRP laminate and steel *Geometry:*Double-strap joint (plates)	To assess how sub-zero temperatures of between −40 and 20 °C affect the bond between CFRP and steel and subsequent bond strength and failure mode.	Results with Araldite® and Sikadur® epoxies in both studies suggested negligible bond strength difference after exposure, but Mbrace® Saturant epoxy results showed a 40% decrease in bond strength after −40 °C exposure. Most common failure type was cohesive failure in adhesive layer, resulting in interfacial debonding.
Nguyen TC et al [35]	Civil	*Material:* CFRP laminate and steel *Geometry:*Double-strap joint (plates)	To assess how elevated temperature of between 20 and 60° affect the bond between CFRP and steel and subsequent effective bond length, stiffness, strength, and failure mode.	For temperatures between 20 and 50 °C, effective bond length increased from 40 mm to 100 mm. Stiffness decreased by 20% at the glass transition temperature (T_g), 50% at 10 °C above Tg, and 80% at 20 °C above Tg. Ultimate tensile strength decreased between 40° and 50 °C by 10–15 and 50% respectively. Lower temperatures led to CFRP delamination, temperatures above Tg led to cohesive.
Liu et al [36]	Civil	*Material:* CFRP laminate and steel *Geometry:*Double-strap joint (plates)	To look at the short-term elevated temperature characteristics of different composite layer numbers.	One-layer thicknesses led to much higher strain than three layers. Furthermore, as temperatures rose to 50 °C, bond strength across all layer numbers decreased by 40%. This was explained to be by larger air pockets in the matrix due to higher temperatures. Also, one sheet joints showed longer effective bond lengths than three sheet joints
Corrosion and Moisture Absorption				
Shanhua Xu et al [37]	Civil	*Material:* CFRP and steel *Geometry:*Double-strap joint (plates)	To assess the effect that steel surface corrosion has on the bond between it and CFRP	It was found that as levels of corrosion increased in the samples, failure changed from adhesive failure to cohesive failure. Beyond this upper point, the failure would return to adhesive failure as total corrosion led to a peeling off effect. Ultimate load values increased in samples with a mass loss of 15% and above (greater corrosion). Greater corrosion also led to a more rapid decrease in shear stress beyond the loaded end.
Ocaña et al [38]	Automotive	*Material:* Epoxy and Polyurethane adhesive and aluminium *Geometry:* Adherend plates and dog bone	Effect of environment and high temperature oil immersion on the joint and bulk adhesive mechanical properties.	The epoxy adhesive showed better performance overall after environmental exposure, with a 6% bending and 3.5% tensile strength increase and decrease respectively, compared to Polyurethane's 11.8% bending and 10.5% tensile decrease. For 80 °C oil immersion, epoxy showed no bending or tensile strength reduction after 128 h, compared with a 50% bending and 35% tensile reduction for Polyurethane.
Oudad et al [39]	Aerospace	*Material:* Epoxy adhesive *Geometry:* 4 mm thick layer	Effect of humidity and the corresponding absorption on adhesive mechanical properties.	There was a 58% reduction in tensile strength after 15 days, after which it remains constant as the adhesive reached saturation. Plastic strain showed variation after 10 days with an 18% increase, going to 25% after 30 days. This suggested a decrease in strength and an increase in ductility and potentially durability with immersion.
Coefficient of Thermal Expansion				
Wang et al [40]	Civil	*Material:* CFRP and steel *Geometry:* Single lap joint (plates)	Investigated the effect of temperature cycles from −20 °C to 40 °C on a CFRP/steel bond, looking specifically at CTE discrepancy between the two materials and how bonding performance is affected.	There showed little variation in tensile strength, elastic modulus and maximum strain compared to the control; around 5% after 500 cycles. There was not a significant change in tensile strength in the T1 adhesive, but there was a 9% decrease in elastic modulus after 500 cycles. For Tc, tensile strength decreased by 17% and yet there was little change in elastic modulus. The average ultimate load with the adhesive Tc decreased by 9%. T1 showed little change and varied less than 5%. Furthermore, the Tc adhesive showed 1.4 times higher ultimate load than T1.

(*continued on next page*)

Table 1 (*continued*)

Source	Discipline	Material /Geometry	Purpose	Major findings
Yoshitake et al [41]	Civil	*Material:* CFRP and steel *Geometry:* Single lap joint (plates + H-beam)	Looked at how CTE discrepancy between CFRP and steel affects the flexural behaviour and hence interfacial bonding integrity when exposed to low temperatures down to −20 °C.	Deflection of a CFRP/steel strip increased under cold temperature due to the CTE mismatch. CFRP laminate is firmly bonded to the H-beam even during cyclic temperature variation, and discrepancy in the CTE of steel and CFRP is negligible when looking at load carrying capacity.

with likely aerospace in-service conditions is limited, and the aim of this article is to summarise findings from various engineering disciplines to provide a knowledge base for future aerospace-based research and development.

2. Driveshaft design: windings

The composites discussed in this article are all laminates, in that they constitute individual layers of reinforcement and matrix, or plies. The phrase 'windings' used relates to the fact that these composites are manufactured into shape using filament winding technology, where a continuous fibre tow is wrapped around a mandrel in alternating directions. The impregnation of the fibres with resin (epoxy, polyester and bismaleimide (BMI) [42] for example) can occur either just before winding (wet winding), after winding, or by using prepreg materials (dry winding) [43]. Studies on other techniques to manufacture such composite driveshafts are rare, however, **Capela et al** [44] and **Pater et al** [45] used vacuum bag moulding and rotary compression respectively, with the latter claiming it as a reasonable alternative from conventional methods. This process occurs at an angle to the length of the shape, so that each ply may have a reinforcement at a different angle to the transverse line and will be repeated until several layers of composite are created.

Layer numbering usually begins at the inner-most or bottom layer. There may exist a mid-plane line, that composite layer designs often form symmetry about when looking at a cross section of the material (Fig. 1) [46].

The windings can be manufactured in alternating angles to create a material with differing material strengths in certain directions. For example, [47] looked at how winding angles from 0° to 90° effected varying mechanical properties of a composite tube, with results altering depending on fibre type (carbon, aramid, E-glass); one case showed radial deformation performance was worst at approximately 20°, 45° and 35° degrees winding respectively, down from the optimum 0° and 90°. Furthermore, circumferential, or hoop, helix, and polar winding layers are often used to describe different laminae orientations. Hoop is most often used for near 90° orientations, perpendicular to the 0° axis, and helix is most often used for ± 45°, although can range from approximately 25° to 85° to the axis rotation (Fig. 2) [48,49]. Polar describes generally the addition of near 0° winds that extend over each end of the shaft, or from pole to pole [50,51] removing the need for repeat passes required with the helix winding.

Classical lamination theory (CLT), used in [10,14], is a theoretical tool that offers a way of calculating stress and strain in a laminate material, considering different loading conditions, as well as calculating loads that will cause first ply failure. It uses the stacking sequence (lamina orientations and its position in the laminate) and other material properties [46].

It is often useful to find the dimensions of a thin hollow shaft required to withstand a certain load. For this, and an equation (1) can be derived from the simple theory of torsion [52], of which the angle of twist can usefully be calculated from, and from which equation (2) can be extracted.

$$\frac{T}{J}=\frac{\tau}{R}=\frac{G\theta}{L}\# \tag{1}$$

$$T=\frac{\pi}{16}\frac{\left(D^4-d^4\right)}{D}\frac{f_s}{2f_{os}}\# \tag{2}$$

For equation (1), T is the torque, J is the polar moment of inertia, τ is the shear stress set up at radius R, G is shear modulus, θ is the angle of twist and L is length of shaft. For equation (2), D is the outer diameter, d is the inner diameter, f_s is maximum allowable stress and f_{os} is the factor of safety.

Poul R et al. [10] compared the design of different driveshafts for connecting a piston engine with an ultralight aircraft propulsion system under torsion testing. The three designs included one aluminium alloy (Al) only, and two hybrid designs with carbon fibre composite central shafts and Al flanges. The two hybrid versions differed through the inclusion of a high-modulus carbon fibre layer. The Al flanges were attached to the composite with a Spabond 345 epoxy adhesive bond, which was also strength tested under torsion.

The Al alloy shaft allowed a comparison to a more traditional driveshaft arrangement, where disadvantages include complicated manufacture and difficulty in tailoring properties. The hybrid shafts provide technical simplification despite an increase in manufacturing steps. The lay-up of the composite sections of the hybrid shafts are shown in Table 2. All shafts were kept to similar dimensions for comparability, with lengths of 953 mm, internal diameters of 115 mm and wall thickness of 1 mm.

Design of the hybrid shafts employed the use of CLT, suitable due to the shafts' thin walls, where equation (3) and (4), highlight the dependency of the mechanical properties on carbon fibre orientation.

$$E(\theta)=\frac{E_x}{cos^4\theta+\frac{E_x}{E_y}\times sin^4\theta+\frac{1}{4}\left(\frac{E_x}{G_{xy}}-2v_{xy}\right)\times sin^2(2\theta)}\# \tag{3}$$

$$G(\theta)=\frac{E_x}{\left(1+2v_{xy}+\frac{E_x}{E_y}\right)-\left(1+2v_{xy}+\frac{E_x}{E_y}-\frac{E_x}{G_{xy}}\right)\times cos^2(2\theta)} \tag{4}$$

where E is the Young's modulus of the composite, G is the shear modulus of elasticity, v_{xy} is the poisson's ratio and θ is the angle between fibre direction and chosen axis of material. Subscript x represents the longitudinal properties, or 0° and 180° to reinforcement and subscript y represents the transverse properties, or 90° and 270° to reinforcement.

All shafts were tested with a torsional moment, with the hybrid shaft designs expected to withstand 500 N·m. CLT software, LamiEx V3, was used to calculate stresses, deformations and effective moduli of elasticity, and Puck's failure criterion [53] was applied on calculated stresses to check if failure occurs when maximal torsional moment is applied.

One of the goals of the study was to design a shaft with a low enough torsional stiffness to require the lightest metallic couplings possible, and so bending and torsional stiffness of all shafts was then calculated using these values, results for which are given in Table 3. It concluded that with a medium longitudinal stiffness, highest torsional stiffness and weight, the Al shaft lost out to the hybrid shafts overall. Version 2 showed relatively low axial stiffness but had a torsional stiffness that was too great, and therefore version 3 was the preferred shaft design. Here, while the HMC provided greater tensile stiffness, it resulted in a lower torsional stiffness. This is because when HMC fibres are all

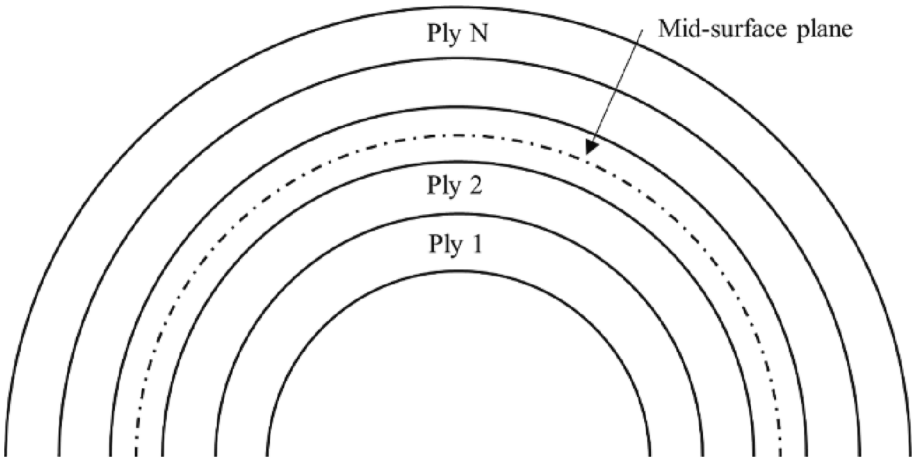

Fig. 1. *Stacking sequence and nomenclature, .*
adapted from [46]

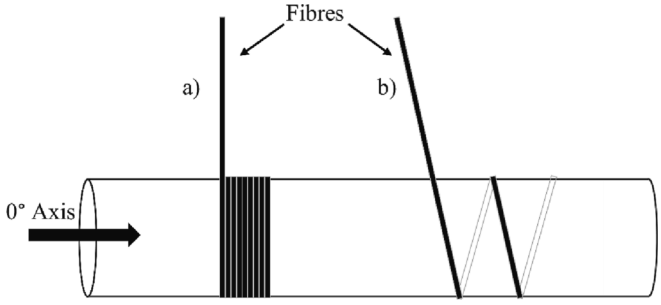

Fig. 2. A) Hoop winding b) helix winding.

Table 2
Layup of the composite sections in the hybrid driveshaft versions 2 and 3; high strength carbon (HSC) and high-modulus carbon (HMC), .

Shaft Version	Lay-up
2	HSC [±45/0/±45]
3	HSC, HMC, HSC [±34/0/±85]

adapted from [10]

oriented in the direction of the tensile load, the composite stiffness is entirely dependent on the stiffness of the fibres. However, when looking at the torsional effect, the stiffness is dependent on a combination of properties from both the fibre and matrix and the interaction between them.

Nayak et al. [5] studied the effect of replacing steel with CFRP and aluminium flanges in an all-terrain vehicle driveshaft. Torsional strength was assessed and compared between the two and failure mechanisms of the CFRP shaft were identified with SEM micrographs.

The CFRP matrix was epoxy resin, with the carbon fibres arranged in a winding pattern of $[85_2/\pm45_2/25_2]_S$, with the composite manufactured using filament winding technology [46].

For torsional testing, metal inserts were bonded to the shaft using Araldite® AV 130 M adhesive, replicating the aluminium flanges which will transfer the torque to the engine via splines attached. A constant test rate of $0.5^\circ \bullet sec^{-1}$ was used. The results from the CFRP shaft suggested an 8.5% increase over steel shafts in average torsional strength; increasing to 1770 N·m from 1630 N·m. Added to this the CFRP shaft had a weight saving of 60%, leading to a far superior strength to weight ratio of 2212 $N \cdot m \cdot kg^{-1}$ compared to 652 $N \cdot m \cdot kg^{-1}$ for steel.

SEM imaging (Fig. 3) revealed that there was good matrix coverage on fibres in general with delamination determined as the main reason for failure, although evidence of resin rich areas and outer-surface cracking was found that would likely have led to a lower torsional strength.

Tariq M et al. [14] investigated how outer layer orientation effected the torsional properties of hollow composite shafts. Inner layer orientation and number of layers was also investigated. Maximum torque, torsional strength, torsional stiffness, angle of twist, and hardness were investigated. The different outer winding layers included hoop and helix.

Three shafts were designed through computer-aided design, with a length of 300 mm and an internal diameter of 20 mm. 12 K carbon fibre tow was used with fibre diameter at 7 μm to 8 μm. The lay-up design was an alternate sequence of 90°-to-axis hoop and ± 45° helix layers. This decision was based on the fact that when torque is applied to a shaft, shear stresses are produced in fibres at 45°. The alternate sequencing was to maintain structural stiffness, circumferential strength, and shear strength. The shafts A, B and C have their details listed in Table 4.

The testing involved measuring the maximum torque that each shaft could withstand and the angle of twist at rupture, done by clamping on the shaft end whilst torque was applied on the other. The results of the testing are approximately summarised in Table 4. The test results concluded that, firstly, Sample B had the greatest torsional strength, followed by Sample C at 27% less and Sample A at 69% less. This was explained to be because of the increase in thickness and the extra helix winding layer. This contrasts with Sample C as it has a lower strength yet

Table 3
Calculated mechanical properties of all shafts, .

Mechanical Property	Axial Young's modulus (GPa)	Transverse Young's modulus (GPa)	Shear modulus of elasticity (GPa)	Axial stiffness ($N \bullet mm^2$)	Torsional stiffness ($N \bullet mm^2$)	Mass (g)
Al alloy only	73.0	73.0	28.0	4.4×10^{10}	3.3×10^{10}	1564.0
HSC/epoxy	63.8	9.8	21.5	4.3×10^{10}	2.9×10^{10}	923.0
HSC + HMC/ epoxy	182.7	39.0	5.1	1.1×10^{11}	5.9×10^{9}	916.0

adapted from [10]

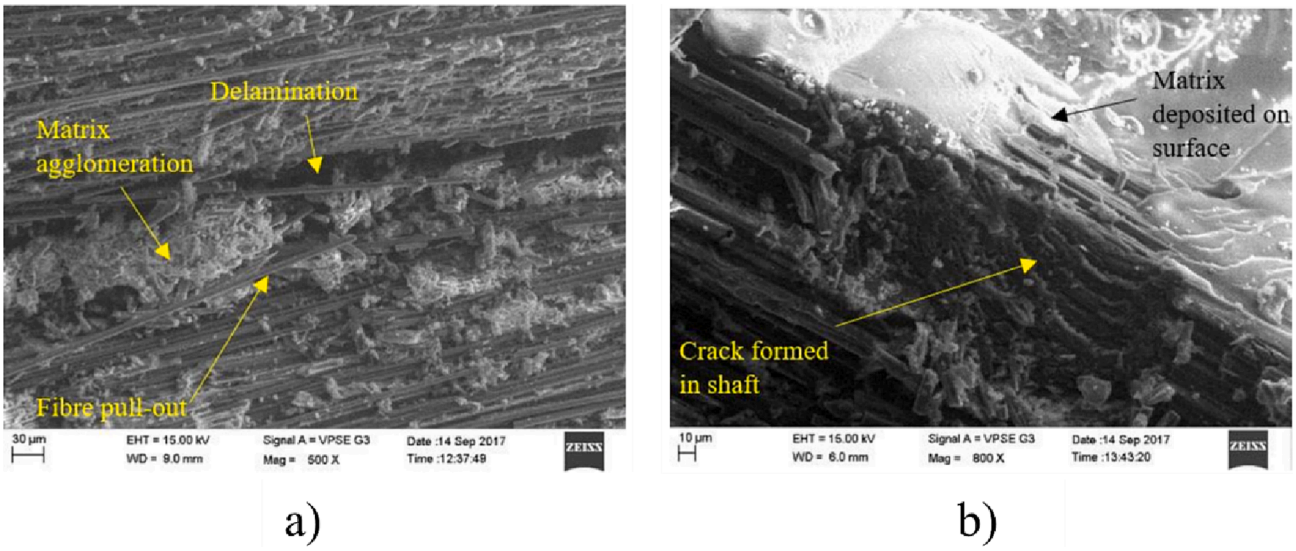

Fig. 3. SEM imaging showing a) resin rich areas but generally good fibre coverage and b) surface cracking [5].

Table 4
Torsional characteristics of different samples, .

Sample ID	No. of Layers	Outer Layer Type	Layer Orientation Θ°	Torsional Strength (N·m)	Torsional Stiffness (N·m·rad^{-1})	Hardness (Hv)
Sample A	3	Hoop	[90/±45/90]	86	380	315
Sample B	4	Helix	[90/±45/90/±45]	205	880	380
Sample C	5	Hoop	[90/±45/90/±45/90]	148	980	315

adapted from [14]

higher thickness and was explained to be due to hoop winding offering less resistance than helix winding, leading to increased thickness without the increase in shear stiffness required. Secondly, angle of twist data shows a correlation between thickness and the amount of twist; that is, the greater the thickness the smaller the angle, and hence the higher the stiffness. Next tested was torsional stiffness, which is described as 'the ability of a material to resist deformation and particularly in case of shafts, it's resistance to rotation'. The equation (5) used for torsional stiffness, k, is as follows:

$$k = \frac{T}{\theta}\# \tag{5}$$

where T is the torque and θ is the angle of twist. Sample C showed torsional stiffness 11% more than Sample B and 62% more than Sample A, again explained by the increased stiffness due to the increased thickness. It was determined that adding a helix layer offered the biggest positive affect at 57%, compared to a hoop layer's 11% when considering individual contribution to torsional stiffness that the different layers had. **Montagnier et al** [54] supported this, suggesting ± 45° plies should be used in order to maximise torque resistance.

Further testing to determine the hardness of each shaft was carried out using the Vickers hardness testing. From the results, Sample B showed the greatest hardness in the helix winding outer layer, compared to the hoop winding in the other two samples. This was found also by **Gupta et al** [55], where natural fibre composites oriented at 45° gave the highest hardness results. The other two samples showed equal hardness, highlighting the direct link between winding pattern and hardness.

The addition of hoop winding is, however, crucial for the circumferential structural integrity, suggesting hoop winding should be left included in a shaft design when buckling strength is the main concern. This becomes apparent when looking at equation (6) [56], which represents critical buckling torque T_{cr} in an orthotropic thin-walled tube, that is significantly affected by hoop stiffness:

$$T_{cr} = \left(2\pi r^2\right)(0.272)\left(E_x E_y{}^3\right)^{\frac{1}{4}}\left(\frac{t}{r}\right)^{\frac{3}{2}}\# \tag{6}$$

Where E_x and E_y are the stiffness modulus in the axial and hoop direction respectively, t is the tube thickness and r is the mean radius. This is supported by [57], which utilised a $[45/\text{-}45/0/\theta]_n$ stacking sequence, and included a mix of glass and carbon fibres in the following layup: [G/G/C/G]. The shaft was 1730 mm in length and had a mean radius of 50.8 mm. Here, the best-case shaft layup for buckling torque was found in modelling to include a hoop outer layer, with increases over a 45° outer layer of approximately 38%. This was explained to be due to 0° (polar) fibres increasing axial strength, and 90° fibres increasing hoop, and therefore shear buckling strength. Furthermore, [58] looked at a glass-fibre wrapped aluminium shaft, with a metallic inner diameter of 40 mm, 1 mm thickness and 300 mm length. For all three FRP thicknesses tested (1 mm, 2 mm, and 3 mm), it was suggested here also that buckling torque capability reduced as the outer orientation layer reduced from 90° to 45°, with [54,59,60], suggesting hoop plies should be used far from the middle surface to maximise torsional buckling torque capability. The studies [56,61,62] also present data agreeing that using 90° ply orientation in carbon and graphite fibre composite driveshafts more generally can increase their buckling torque limit over 45° by 14.5%, 52.5% and 59.4% respectively.

Outer helix winding could then be deployed when tasked with increasing thickness for improved stiffness, although **Tariq et al** [3], as mentioned later, contradicts this.

Sun Z et al. [15] investigated the natural frequency and damping of CFRP driveshafts, focussing on assessing the effect of ply angle and thickness, whilst comparing drive shafts with and without metal flanges, with and without the flange transition zone and comparing flanges that are both glued and embedded using filament winding. A design technique was proposed to mitigate hidden dangers such as fatigue and high

hydrothermal characteristics found during operations [63,17]. This work stemmed from the lack of research into natural frequency and damping properties of CFRP drive shafts with flanges and looked to validate the use of finite element analysis (FEA) in accurately modelling and predicting the natural frequency of CFRP tubes.

FEA and pulse vibration excitation technique (PVET) was used to compare the drive shafts' natural frequency and damping response at 12 different ply angles and thicknesses, with and without flanges. Furthermore, to simulate a composite tube for FEA comparison and validation, the flange and transition area were cut away to create specimens. Finally, the effect of the transition area on the CFRP drive shafts was determined.

The CFRP drive shafts were manufactured using filament winding technology, where layer thicknesses was 0.3 mm. The outermost layer was wound at 90° (hoop) for radial tension. Each flange was directly integrated into the CFRP tube during winding. FEA modelling ignored the transition zone complexities and instead assumed a uniform fibre angle. Experimentally, a free-free modal test was used, PVET, where an impulse hammer impacted points along the shaft, with vibration responses detected by an accelerometer.

FEA suggested the natural frequency of CFRP tubes decreased by 62.71% with an increase in ply angle from 15° to 65°. Results from PVET showed a 63.35% decrease with an increase in ply angle from 15° to 65°. These results (Fig. 4) suggested a high importance of ply angle on natural frequency, but also that the FEA results were valid.

When comparing with or without a flange, a reduction in the natural frequency was found but with no influence on the relationship between natural frequency and ply angle. The small difference in FEA and PVET was explained by the omission of a transition zone in the FEA.

PVET determined that the larger winding angle, the shorter the vibration period and hence the greater the damping. Moreover, measured natural frequency showed to be only slightly lower than calculated natural frequency by theoretical formula, indicating that the transition area did not affect the natural frequency.

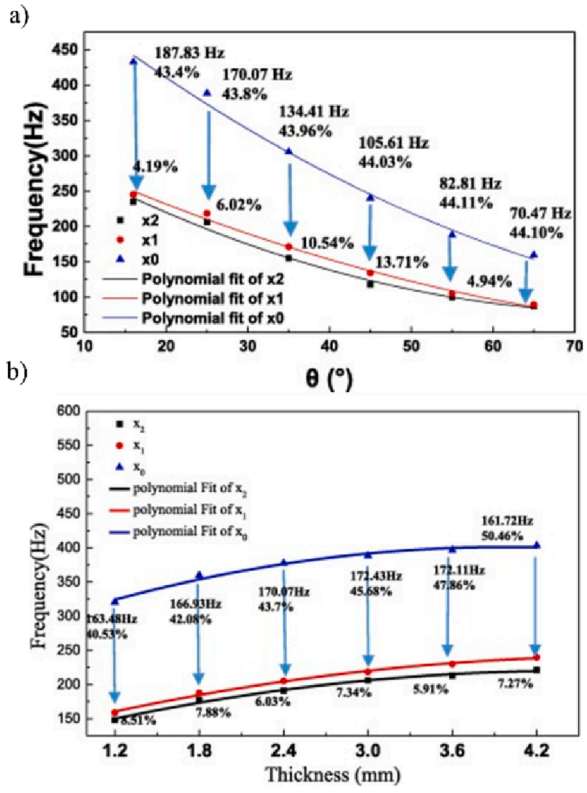

Fig. 4. A) Changes in natural frequency with ply angle. x0. cfrp by fea, x1. cfrp drive shaft by fea, x2: cfrp drive shaft by filament winding technology by pvet. b) changes in natural frequency with thickness. x0: cfrp tubes by fea, x1: cfrp drive shaft by fea, x2: cfrp drive shaft by pvet [15].

Number of plies included 14, 12, 10, 8, 6 and 4. FEA was used to calculate vibration modes, and the CFRP tubes' natural frequency decreased overall by 20.53% over the ply decrease from 4.20 mm to 1.20 mm. Likewise, CFRP drive shafts with flanges had a natural frequency decrease of 33.79% over the ply decrease from 4.20 mm to 1.20 mm (Fig. 4). When comparing this with ply angle, ply thickness has a greater influence on natural frequency: 33.79% compared to 20.53%. PVET results showed a similar trend with a deviation of 7% due to omission of damping factor and transition zone.

As before, impact acceleration suggested that the greater the winding thickness, the higher the damping. Other studies [64,65], however, reveal the positive effect of thinner ply thickness on shaft characteristics such as fatigue life and ultimate strength, with thinner plies being up to 150% stronger. Therefore, a compromise between damping characteristics, fatigue life and strength must be found in the development of future driveshafts.

Prasad AS et al. [16] looked at the design of a two-piece E-glass/Epoxy composite driveshaft with integrated metallic joints for automobiles, choosing an optimal stacking sequence to meet design specifications of static torque capability and bending natural frequency. A comparison was then made to a more standard mild steel-only shaft.

The composite shaft with metallic joints was designed with a torque capability of 1500 N·m, similar to the steel shaft with equal dimensions of length and outer diameter. The simple theory of torsion [52] and hence it's derivative for a hollow shaft (equation (2)) were used to find the angle of twist and inner diameter respectively. The natural frequency, fn was determined using equation (7), where E is elastic modulus of the E-glass/Epoxy, I is moment of inertia, m is mass of shaft and L is length of shaft.

$$fn = \alpha^2 \times \sqrt{\frac{EI}{ml^4}} \tag{7}$$

Two common stacking sequences were first suggested: $[90/\pm15/\pm54.7/\pm75/90]_s$, and $[90/0/\pm45/0/\pm45/90]_s$, before the stacking sequence $[15/\pm54.7/\pm75/90]_s$ was chosen; an omission of a 90° hoop layer was explained to be for the overall thickness to be below 9.5 mm to have an equivalent torsion to the steel shaft, since the shear modulus of fibre reinforced composites are lower than steel [66,67]. The shaft was manufactured using filament winding technology, and the thickness of each layer respectively was 1.2 mm/1.2 mm/1.2 mm/0.5 mm.

The overall weight and thickness decreased when using glass epoxy by 38% and 36.6% respectively, decreasing the sprung mass and reducing vibrations and fuel consumption. The torque bearing capacity of the composite driveshaft was increased by 75% when directly comparing to the steel shaft. Moreover, the composite driveshaft was found to withstand 10.5% higher buckling torque, with 25.7% higher stiffness and 25% higher natural frequency than the steel shaft.

Sevkat et al [17] investigated the effect that both lay-up sequence and torsional strain-rate have on the torsional behaviour of hybrid reinforcement composite driveshafts.

Both carbon fibre (C) and E-glass fibre (G) were used as reinforcements, with all three test shafts consisting of two glass and two carbon fibre layers, at a winding angle of [-45/+45], with an epoxy matrix. The shafts had the following layer orders from inner to outer diameter: [G/C/G/C], [C/G/C/G] and [C/C/G/G].

For torsion testing, square steel tubes were attached at either end of the composite shaft using an interference fit, with the steel having inner dimensions equal to the outer diameter of the composite tube. This 'gripping' method was at first tested on aluminium/glass fibre shafts in this same study, where 1500 N•m was achieved; maximum torque of the composite shafts was predicted to be in the range of just 150 N•m to 200 N•m, so this technique was approved.

For the static testing of different stacking sequences, a test rate of

Table 5
Stacking sequence effect on max torque and twist angle tested at 0.1°/s, .

Stacking sequence	Maximum torque (N·m)	Maximum twist angle (°)
G/C/G/C	175	5.24
C/G/C/G	155	5.52
C/C/G/G	145	5.9

adapted from [17]

$0.1^\circ\ s^{-1}$ was used. To assess the effect of loading speed, the standard $0.1^\circ\ s^{-1}$ was compared with $5^\circ s^{-1}$.

The results of altering the stacking sequence are highlighted in Table 5. During the tests, shear stress decreased linearly radially, with the highest stresses near the surface and none at the centre. Results suggested that if carbon fibres were used in layers with high shear stress, such as the outer layers, a higher torque could be achieved. Using glass fibres in these outer layers offered a higher maximum twist and therefore ductility. This is because while carbon fibres are stiff, they are also brittle, and so while torque resistance increases with carbon fibres, ductility is reduced [68]. This effect is reinforced by [69], that looked similarly at a hybrid reinforcement of carbon and E-glass fibres using ANSYS modelling. Here, a carbon fibre layer was introduced to replace one of the four E-glass layers in an automobile driveshaft, moving from inner to outer diameter. As this occurred, there was a very small negative effect on torsional shear stress (+0.56%), and a positive effect on strain (-21.70%) and buckling torque (+26.00%) capabilities. These results open the possibility of adjusting stacking sequences of carbon and glass reinforcement to gain desired mechanical performance of driveshaft.

When looking at loading speed, the 5°/s loading rate showed a decrease in twisting angle compared with 0.1°/s across all three shaft types, but with maximum torque staying largely the same, suggesting very high torsional speed on composite shafts do not jeopardise their torsional strength. This contradicts a study by **Naik et al** [70] which suggested, using a torsional split Hopkinson pressure bar (TSHB), that a high torsional speed has a positive effect on shear strength. For example, a plain weave carbon/epoxy composite gained a 67% increase in shear strength at 1000 revolutions per second over quasi-static loading. This was explained to be due to the lack of time for any damage to propagate through the material. This discrepancy should be investigated further, but may be as a result of TSHB testing errors due to the various assumptions that need to be fulfilled in order for the test to be representative [71].

Tariq et al [3] investigated the torsional performance, chemical reactivity, hardness and density of a composite driveshaft, manufactured utilising different individual fibre reinforcement types in each of the layers, rather than individual reinforcement changes across layers, where results could then be compared to a pure carbon fibre counterpart.

The different reinforcement mixes included carbon/glass and carbon/aramid, and a comparison was made between room and high temperature cured epoxy, Epolam 2040 and Araldite® 564 respectively. The use of aramid fibres, or commonly Kevlar®, is being seriously considered in future aerospace endeavours for its high strength, modulus and temperature capabilities [72]. The Araldite® was cured at 150 °C. Using validated FEA in ABAQUS, an ideal lay-up was decided upon, as it was found that adding a ± 45° helix rather than a ± 90° hoop layer enhances torque by 75% to 85%, and that helix layers provided 30% to 40% more torsional strength when on the surface than between thicknesses. Also, alternating sequences in layers gave 30% to 40% greater torque compared with an agglomerated sequence of layers. As a result of this, a [Y/X/Y/X/Y] sequence was chosen, where *Y* indicated helix, and *X* indicated hoop layers. In total, six shafts were manufactured, with pairs of each reinforcement type, each cured at either room temperature (RT) or 150 °C.

Test procedures included torque testing for maximum torque using ASTM E-143, Vickers hardness testing using ASTRM E-384, density measurements using a water displacement method and ASTM D792-13, chemical reactivity testing through submerging the samples in both 3.5% saline solution and 98% H_2SO_4 and measuring dry weight change.

Torsional testing results are shown in Fig. 5. Glass and aramid fibres decreased torsional properties by 43% and 23% respectively compared the carbon fibre composite condition. Furthermore, RT cured epoxies gave improved torsional properties of between 8% and 17% for all three shaft compositions.

No degradation of the shafts was found after saline submersion, but

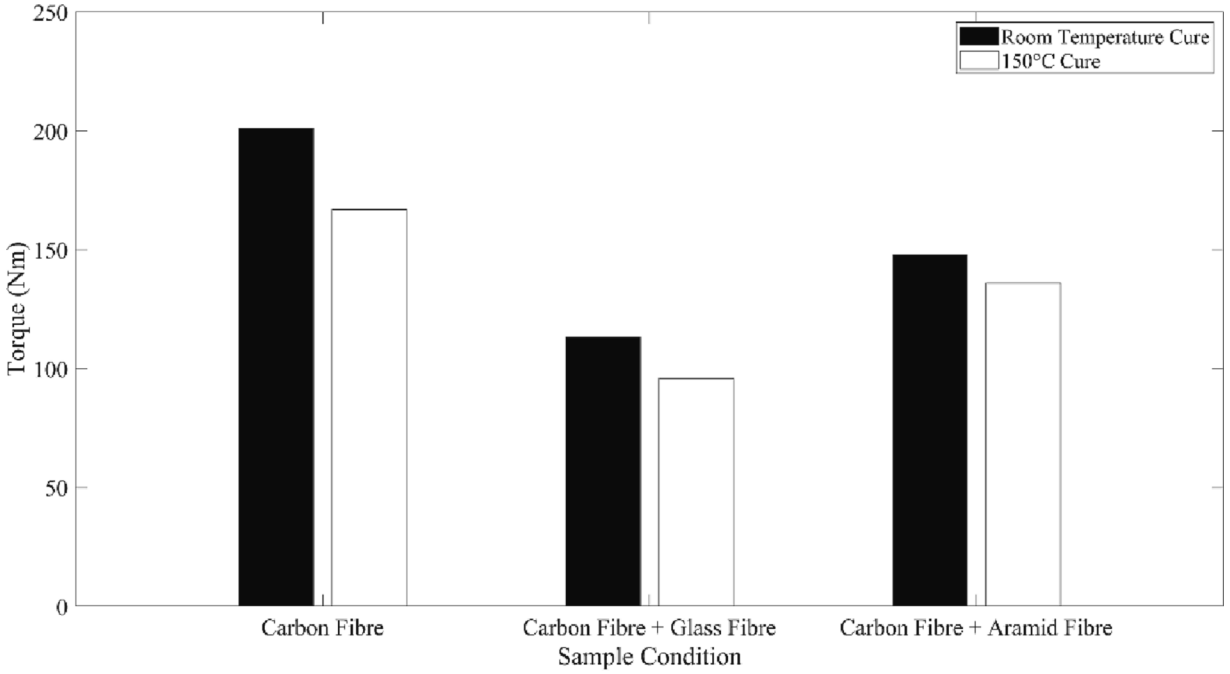

Fig. 5. Torque values for 1) Carbon fibre 2) Carbon fibre + Glass Fibre 3) Carbon Fibre + Aramid Fibre, with either a room temperature or 150° cured resin, . adapted from [3]

carbon-aramid composite shafts showed 20.8% weight loss after acidic immersion, as opposed to carbon fibre only, losing just 6.2%. Both values were with RT cured epoxy, performing worst overall. This poor performance of the carbon-aramid shafts can be explained by the acids leading to hydrolysis of both the epoxy and the aramid fibres [73]. Up to an 83.4% reduction in the tensile properties of an aramid fibre reinforced polymer after 288 h immersion in a 30% concentration sulphuric acid was found in [74], and suggested that whilst a tensile reduction was slower in saline water, it does occur after an extended period of time. Similar results were found in [75,76] but suggested a higher impact from saline water. The shafts with hybrid reinforcement appeared more resistant to mechanical wear after hardness was seen to increase compared to carbon fibres only from between 12.0% and 14.7% for glass fibre and aramid fibre respectively, with the RT cured epoxies showing the greatest hardness. Shown also in [77,78], where aramid fibre impact resistance was compared to and exceeded carbon fibre, it was explained to be due to the increase of ductility and extensibility in the aramid fibres. Finally, the carbon-aramid shaft showed the greatest weight saving at 10%, with the specific strengths as follows in Fig. 6. Whilst it was found that carbon only shafts had superior specific strength values, it can be recommended to use these aramid fibres in certain applications due to their lower weight overall and more significantly their lower cost.

Henry et al [25] looked at a multi-objective optimal design for CFRP rotorcraft driveshafts. For example, traditional metallic helicopter drivelines utilise several segments, held together by couplers and hanger bearings. A simpler, composite driveline would require fewer or none of these parts, and so in conjunction with other design variables such as stacking sequence and laminae number, the following failure criteria were looked: overheating, whirl instability, torsional buckling and material failure. The design goals of lower mass and higher factor of safety were then set.

Results concluded that a reduction in bearing and lamina number in the mid-span region had a negative impact on the whirling and buckling safety factors respectively. Lower fibre angles led to fibre-direction compressive stress. The matrix with the highest modulus of elasticity, EPON 862, used in conjunction with AS4D-GP-12 K carbon fibres, gave rise to the lightest designs, eliminating one bearing. The mass reduction in this case was 15.15 kg relative to the original mass of 31.3 kg in a UH-60 Blackhawk case study [79], which used a majority aluminium driveline and an associated set of five segments with six couplers and four hanger bearings required.

Henry et al [26] then looked at how 7.62 mm and 12.7 mm diameter incendiary rounds impacted the residual strength and stiffness of a CFRP/Epoxy driveshaft, and how this was affected by layup.

Two layups were compared, with differing orientations, thicknesses, and fibre volume fractions (Table 6). The two composite driveshafts had a length of 1420 mm and a 76 mm inner diameter. They were adhesively fastened to the test frame with steel insert flanges. The projectile target was centre to the length of the shaft, and such that it would pass through the outer radius of the shaft. This 'cut' was at 45° to the gun barrel. The 7.62 mm and 12.7 mm rounds had a target velocity of 762 $m \bullet s^{-1}$ and 487 $m \bullet s^{-1}$ respectively..

Whilst, for 12.7 mm rounds, the stiffness was found to be equal across shafts at 13%. It was found, for 7.62 mm rounds, that there was higher damage influence on residual torsional stiffness for shaft 2, at 17% compared to 21% for shaft 1. There were two possible reasons found in previous literature that explain this reduction: larger fibre angle differences between lamina (85° to 30°) [80] and higher fibre angles having lower typical residual strength after impact [81]. The more flexible shaft 1 also propagated less delamination perpendicular to the line of the projectile compared to shaft 2.

Table 6
Composite driveshaft properties, .

	Shaft 1	Shaft 2
Layup	$[\pm 40/\pm 30_3/\pm 35_3]$	$[\pm 85/\pm 30/\pm 35/\pm 40]$
Polar moment of inertia (mm^4)	1.43×10^{-6}	6.72×10^{-5}
Fibre volume fraction (%)	50	65

adapted from [26]

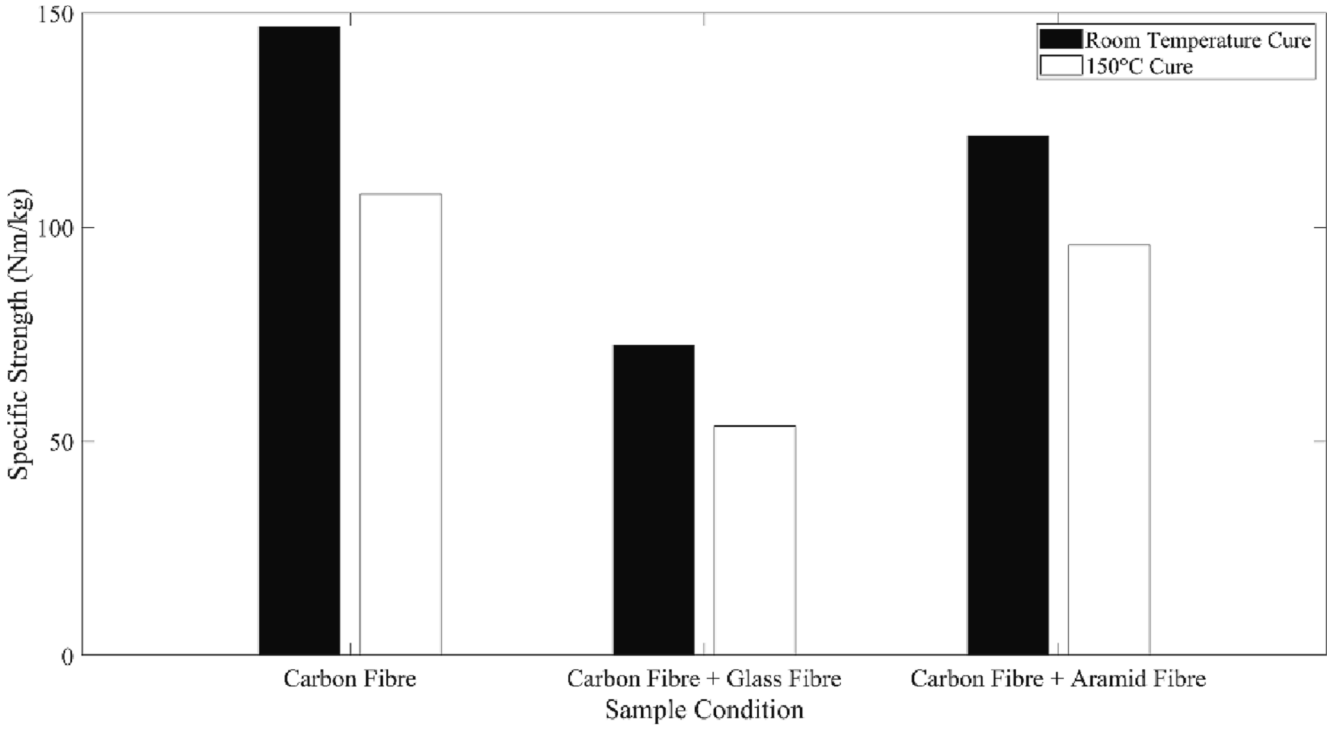

Fig. 6. Specific strength values for 1) Carbon fibre 2) Carbon fibre + Glass Fibre 3) Carbon Fibre + Aramid Fibre, with either a room temperature or 150° cured resin, data .
adapted from [3]

3. Driveshaft design: couplings

The emergence of hybrid composite/metallic driveshafts has its obvious advantages through weight savings, as well as leading to an improved strength to weight ratios, as seen in [5,16,82,83]. For certain components of these driveshafts, however, it is essential they remain metallic due to the difficulty in manufacturing composite parts able to directly transfer torque [84]. An example is this coupling type between shaft and flange, which in accessory drives of aeroengines are often connected via involute splines (Fig. 7) [85] along the outer diameter of the shaft insert, to the flange, also mostly metallic, which has female splines in order to accept the torque. Whilst composite replacement for steel in high stress regions in gearing, like the teeth, is beyond current composite material capabilities, the flange and other intermediary stages (bull gears, planet gears and planet carriers for example [86]) between shaft and gearing have seen composite/steel hybridisation, and are in early-stage development [18]. Weight improvements in this region could lead to even more dramatic weight losses compared to just the hybridisation of driveshafts, whilst reducing noise from the interruption of vibration transmission. The importance of this could be linked with proposed future turbofan designs that lean towards planetary gearsets [87,86], where the weight reduction from fewer stages may be offset by the introduction of the gearbox.

The spline couplings are found also in the torque introducing end fittings, fitted either in or on both ends of the composite shaft, often through an adhesive or, more recently, a spline interference/press fit [88,89] (Fig. 8), allowing the composite shaft to withstand both torsional and axial stresses. The techniques used to attach these inserts to the composite shaft vary, and studies have attempted to optimise this feature using different metal interface shapes [24,22,90] bond thicknesses [24], composite layups [24] and join types [23]. More often, however, a circular shape is used when studying the adhesive bond for simplification.

Testing of these interface types often deploys variations of the single lap shear test, in which two materials are adhesively bonded to each other in parallel and a horizontal force applied. The variations in testing are shown in (Fig. 9). Both single and double lap joints offer identical failure modes, and differ only in giving different ultimate loads, CFRP strain distributions and interfacial shear stress distributions of the bonded interface [91].

The following also builds upon the review of adhesively bonded composite tubular joints by Parashar et al [92].

Laberge et al [18] looked at the validity of composite hybridisation of the couple between driveshaft and bull gear in rotorcraft. Much of the assembly continued to be gear steel, but included an adhesively sealed composite webbing section (Fig. 10), connecting inner driveshaft coupling to the outer bull gear teeth. This composite webbing consisted of three sections, the centre of which transferred torque via a sinusoidal interface from shaft to bull gear. This section is then held in place by the further two composite plates. This design was found to be 20% lighter

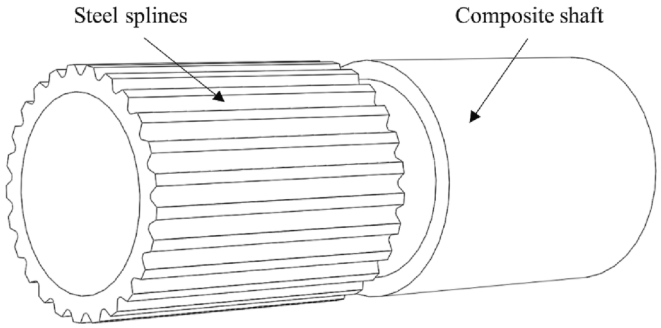

Fig. 7. An involute spline on the outer diameter of an insert for a composite shaft.

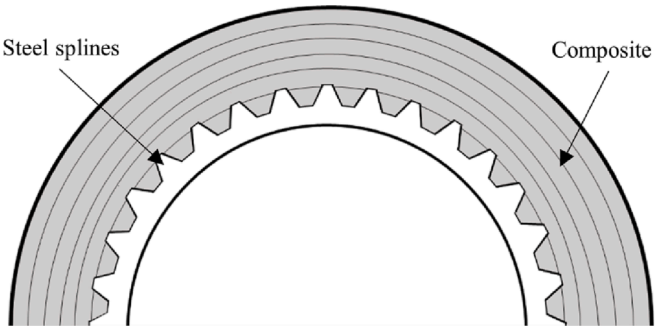

Fig. 8. Axial view. an example of steel splines press fitted into a composite shaft, .
adapted from [88]

than an all-steel equivalent [93].

The composite material used a $[0/\pm 60]_n$ braided prepreg, with T-700 SC carbon fibres and Tencate TC-250 resin. The composite and the Cytec MTA-241 adhesive film bond layer were co-cured. The steel and hybrid versions of the web had a thickness of 14.6 mm and 21.2 mm respectively, chosen to have comparable bending stiffness'.

Testing involved using a high-speed helical gear rig, aiming to replicate operationally similar conditions, using gearboxes that are joined together with input and bull gears via driveshafts. This set up allowed several tests to run concurrently, giving a comparison of different gear configurations before testing, of which a double helical pattern was decided upon to eliminate the axial load seen in single helical gear systems. The testing ran at 49 °C, a conservative starting temperature to test the new product, without risk of composite mechanical degradation. Previous testing had discovered failure in the adhesive bond at 11300 N·m, and so the torque limit here was set to 40% of this. Accelerometers were installed radially and axially, probes were set at 90° out of phase, and thermal data was collected from thermocouples at gearbox oil outlet and inlets. 17 tests were run, with shaft speed ranging from 900 RPM to 5400 RPM, torque from 5000 N·m to 58400 N·m, and power from 53 kW to 3731 kW.

Results were successful in that the hybrid bull gear tested up to 2460 kW, whilst having a weight reduction of 4.5 kg. Vibration saw little change, apart from at 5400 RPM, between 19,300 N·m to 38,600 N·m torque and 1233 kW to 2466 kW power, where axial vibration increased slightly, and radial vibration decreased a similar amount. The hybrid assembly did not affect the overall thermal behaviour of the gearbox.

Further testing by **Laberge et al** [19] looked at the effect of altering the thickness over the radius of the composite section, such that the inner radius gradually decrease thickness towards the outer diameter, by a reduction in ply number, in a 'stair stepped' design. Static torsion testing and testing in operationally similar conditions in the relevant gearbox environment (as before) was used.

Here, the materials used were as before, however the composite thickness began at 16.9 mm at the inner radius, progressing to 10.6 mm at the outer diameter, comparing to a steel example as before.

Static testing was performed at 0.2° min^{-1} until failure or max torque. Digital image correlation (DIC) monitored deformation. The High-Sped Helical Gear Train Rig was used as before, with the same 17 testing conditions.

The torque response from the static testing showed that the hybrid section endured up to 27,100 N·m, at which point the maximum torque allowed by the apparatus was reached. DIC results were taken 30° apart: either above a lobe from the intersecting metal insert, or between lobes. Measurements taken between lobes showed 50% more strain, with this strain decreasing with increasing composite step number from the inner radius. For example, the 3rd composite step showed similar strain to measurements taken 'above lobe'. Overall, the static torsion capabilities of the hybrid section were successfully rated up to 3730 kW, with

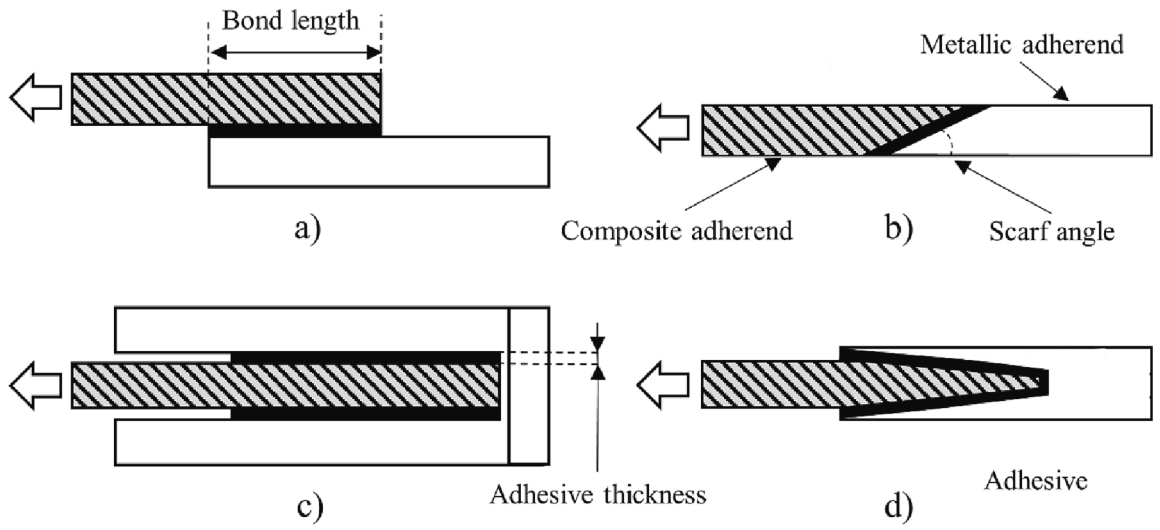

Fig. 9. Cross sections of the following: a) Single lap joint b) single lap joint with scarf c) double lap joint d) double lap joint with scarf.

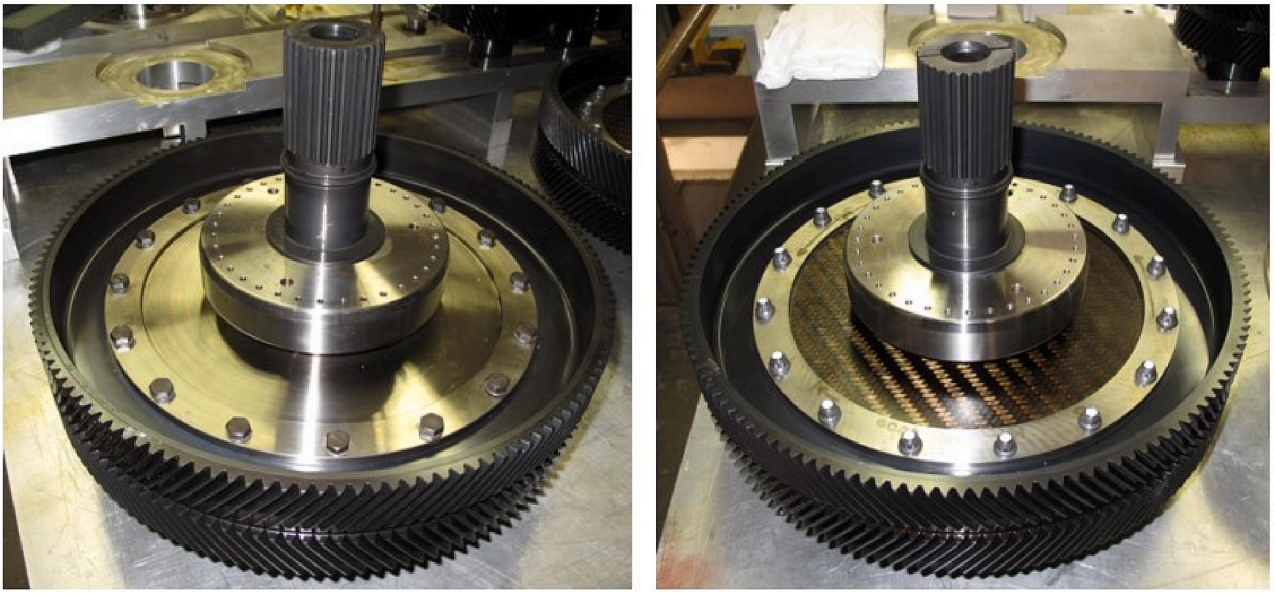

Fig. 10. Bull gear assembly with a) steel and b) composite/steel webs, taken from [18].

maximum strain in the testing rig occurring in the driveshaft. Dynamics results show similar vibration levels for both steel and hybrid designs, aside from at 1030 kW and 1230 kW, where hybrid vibration was slightly larger. Comparing to the non-variable composite thickness hybrid design [18] and above 1030 kW, the temperature difference between fling off and oil inlet was 2 °C to 5 °C higher.

Future research included recommending testing the possibility of a blended web-shaft arrangement, leading to a further weight reduction from lack of bonded interface. This could come about from the advancement in technologies such as automated fibre placement, already enabling an increase in composite structure complexity in aerospace [94].

Furthermore, **Gauntt et al** [20] later studied, through modelling, the effect of altering the composite material properties and layup sequence on a hybrid gear for rotorcraft, comparing to the experimental results of the previous hybrid design shown above [93], and the triaxially braided composite hybrid gear design in [95]. Results showed natural frequencies similar across all composite types, but up to 23.5% below the steel gear for some modes. Although not optimised for weight loss, hybrid samples showed a 14.7% to 18.4% weight loss over the all-steel gear. **Waller et al** [21] also looked at optimising the initial hybrid gear design, mainly to allow for 'oil-off' conditions, where temperatures can rise to up to 232 °C, above most FRP composites functional capabilities. It was found that, over 204 °C, the carbon composite web using BMI resin offered the highest compression strength compared with epoxy. This did come with an associated increase in defects in the BMI resin, as seen in (Fig. 11), a possible result of postcuring. This was seen as an anomaly, specific to the 'resin, fibres, sizing, braided fabric, and/or processing conditions' that were used in the work.

Furthermore, the study compared pitch vs Polyacrylonitrile (PAN)-based fibres thermal and compression properties and found that pitch-based laminates retained a thermal conductivity similar to that of the steel comparison (50 $W\cdot(m\cdot K)^{-1}$ to 60 $W\cdot(m\cdot K)^{-1}$), but had a lower compression strength compared with PAN-based laminates. The study then found that combining both fibre types led to a balance of both properties, but warned that for even load sharing across plies, the modulus of the two types of fibres should be similar.

Kim et al [22] investigated torque transmission capabilities of

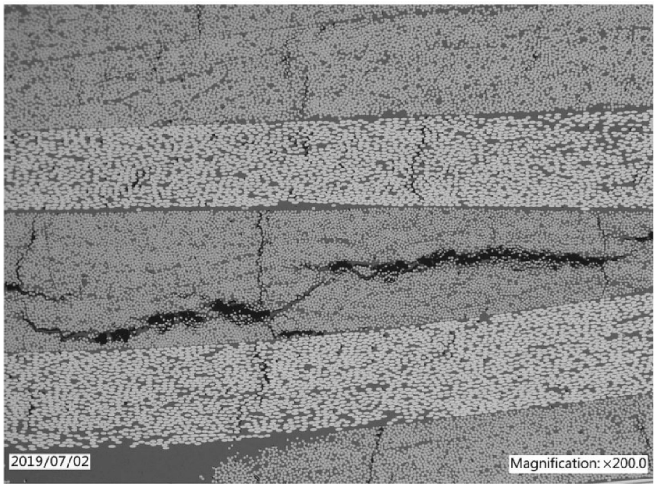

Fig. 11. *Matrix cracking and delamination in BMI resin (post cure), taken from* [21].

composite/steel bonded tubular lap joints with the following different geometries: circular single lap, circular single lap with scarf, circular double lap, circular double lap with scarf, hexagonal single lap and elliptical single lap. Fig. 12 shows an example of the circular nature of most of the lap joints in this study, a technique used to replicate shaft conditions more closely, and the hexagonal composite geometry single lap joint.

The samples used carbon fibre and SM45C steel, with IPCO 9923 epoxy adhesive. The dimensions of the shaft were based on equation (2), using a torque value of 2000 N·m, the required torque for commercial cars and light helicopters, and at $0.5^{\circ}\text{min}^{-1}$. The average diameter and thickness were 60 and 3 mm respectively, with stacking sequences of $[\pm 15]_n$, $[\pm 30]_n$, and $[\pm 45]_n$. It was suggested a smaller angle should be used for higher natural frequencies, and a larger stacking angle should be used for torque transmission capability, as in [58,60]. A 0.15 mm adhesive thickness was used to balance torque capability and achieve a reliable joining operation. The circumference of the elliptical and hexagonal joints were equal to that of the circular joint to ensure the same joining areas.

The results (Fig. 13) suggest that the hexagonal single lap joints had maximum torque capability, with similar results to that of the circular

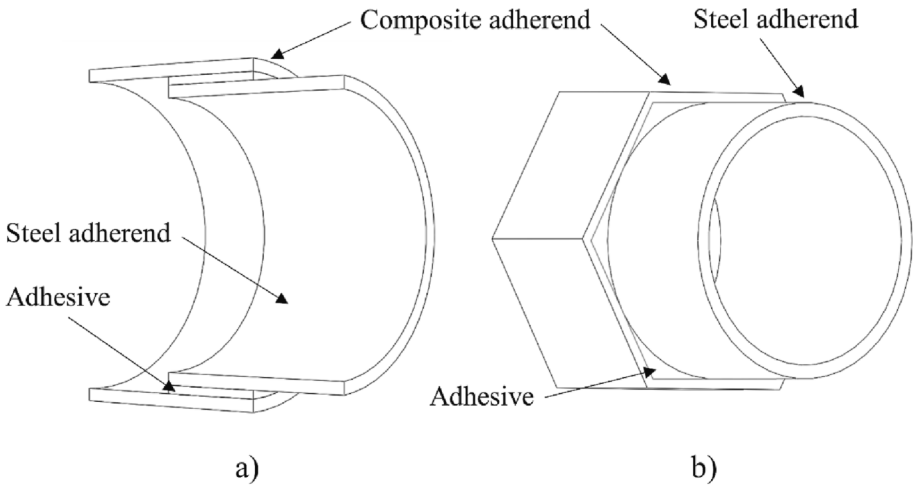

Fig. 12. 3D drawings showing cross sections of a) a circular single lap joint and b) a hexagonal single lap joint.

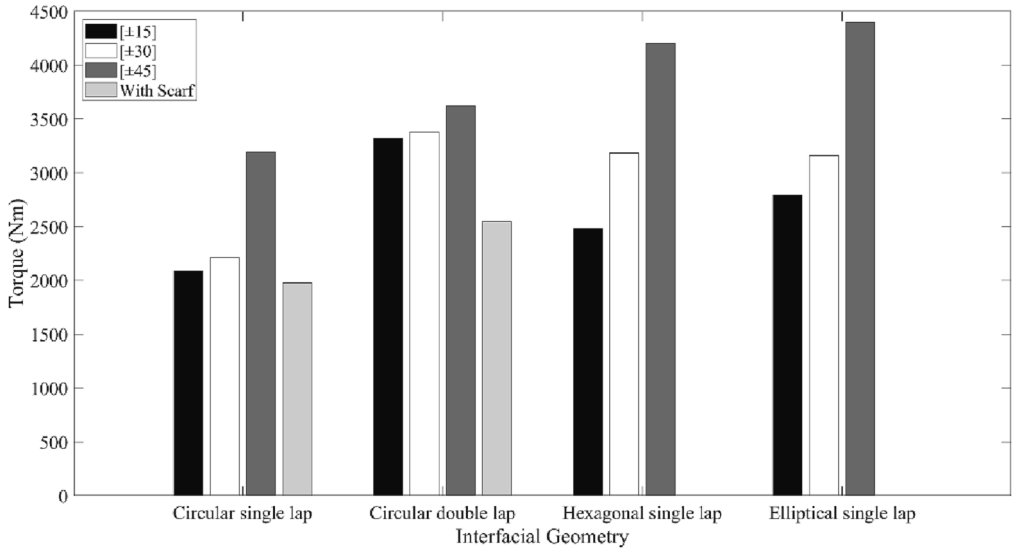

Fig. 13. Torque transmission capabilities of adhesively bonded lap joints with different interfacial geometries and composite lay-ups, . adapted from [22]

double lap joint. Both the hexagonal and elliptical joints had higher capabilities over circular, due to the mechanical effects of their intruding angles into the composite material, providing a greater interfacial contact and hence greater static friction. Furthermore, the circular double lap joints had higher torque capabilities than single lap due to a similar interfacial contact area and prevention of the composite bulging from hoop stresses. Finally, the scarf joints showed no improvement in torque capabilities.

To increase the effectiveness of scarf joints for aerospace applications, **Moreira et al** [96] looked at adding external reinforcements on either one side of, or both sides of an aluminium/aluminium join. The reinforcements consisted of 1 mm thick plate, adhesively bonded at a thickness of 0.2 mm. It was found that adding reinforcements on both sides led to between a 145% to 275% improvement in strength, with scarf angles at 10° to 45° respectively. Improvements such as these should be considered before choosing alternative fixture methods.

Lee et al [23] designed a metallic/composite automotive drive shaft with a static torque capability of over 3500 N·m, a common goal for passenger cars [27,6,7]. The carbon fibre composite layer in this case was positioned inside an aluminium layer to avoid delamination from low velocity impacts or degradation through water absorption. Here, a flange was manufactured with splines on its inner diameter, attaching itself to the outer diameter of the aluminium/composite shaft which runs the length of the shaft, contrary to previous studies which used inserts and were composite only for most of the length. Through press fitting, grooves were engraved onto the aluminium, enabling a mechanical fit with the flange and torque transmission.

This highlighted the importance of correct interfacial behaviour, and it was therefore important to find the optimal protrusion shape, with failure predicting to occur either in stress concentrations at the tips of a serrated, or pointed, spline design, or fretting fatigue with applied torque. Stress concentration was reduced by having smoother splines in a sinusoidal shape, where the aspect ratio of the sinusoid, h_p/w_p was lowered (Fig. 14). FEA conducted on the shaft under 4360 N·m of torque highlighted a relationship between slip amplitude and the height and width of the splines, showing that a slip amplitude of 10 μm could be achieved with an aspect ratio of 0.25. This aspect ratio value led to a width of 0.25 mm, and a height of 0.0625 mm. Any height taller ran the risk of the press fitting operation failing the drive shaft due to the higher loads required, and any width lower would create a spline too difficult to manufacture. Splines were machined without sharp edges to reduce stress concentrations, and a compressive stress was also added to reduce relative movement between the steel and aluminium layers, decreasing fretting fatigue [97].

The average shear stress, τ, of the press fitted joint was also calculated using the following equation (8) [98,99]:

$$\tau = \frac{T}{2\pi r^2 L}\# \tag{8}$$

where T, r and L represent the torque capability, radius and fitted length of the press fitted joint, respectively. Here, the average shear strength of the protruded joint was 34 MPa, 1.5 times higher than of a similar adhesively bonded joint without protrusions [27].

The carbon fibre used was USN150 and was proceeded in manufacture by a glass fibre epoxy UGN150 that was laid up on the inner surface of the aluminium tube to protect against galvanic corrosion between the aluminium and carbon fibre composite. The carbon fibre stacking angle was 0° from the shaft axis for highest elastic modulus in the axial direction, and four 0.5 mm plies of carbon fibre composite were used. For the glass fibre composite, a crowfoot satin prepreg was stacked at 90°, due to high compressive thermal residual peel stress in the thickness direction.

Torque testing used a shortened 250 mm length of aluminium/composite, as opposed to the full 1.32 m length designed shaft, with the steel outer flanges on either side still. The shaft gave a maximum torque value of 4320 N·m at angle of approximately 19°. Neither delamination failure or protrusion failure was found before buckling, however, failure of the protrusions on the aluminium tube were imaged at 100x (Fig. 15) after buckling and disassembling, showing the peak of the protrusions flattened. These were estimated to have a theoretical torque capability

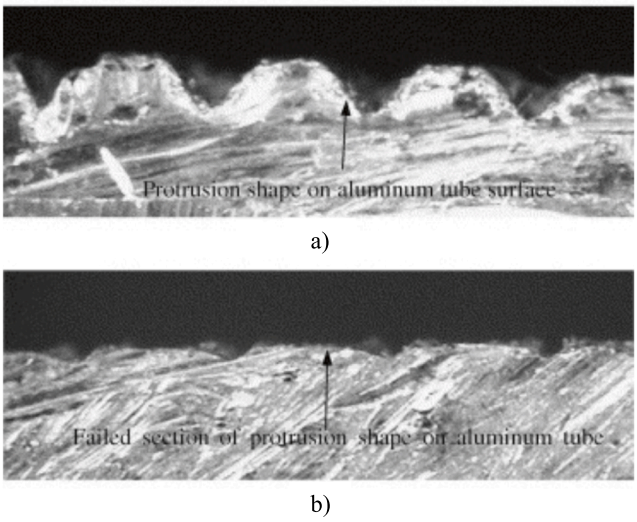

Fig. 15. Microscope view of protrusions at 100x: (a) section view before failure; (b) section view after failure, taken from [23].

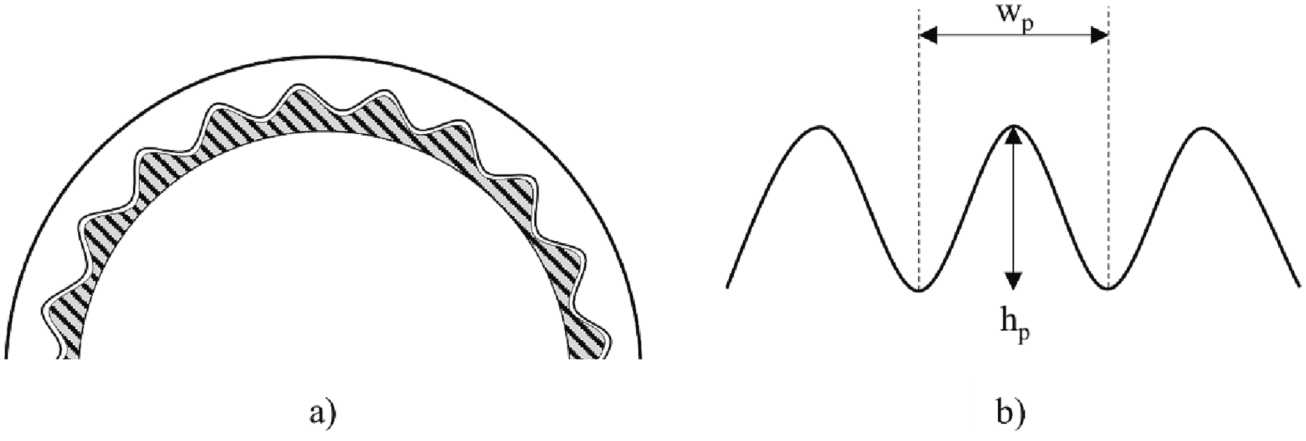

Fig. 14. Schematic of a) sinusoidal spline interface in press fit joint b) sinusoidal aspect ratio h_p/w_p.

of 4360 N·m, and it was explained to be due to the buckling failure of the aluminium tube that decreased this value to 4320 N·m.

Choi et al [24] *studied the effect that adhesive thickness and stacking sequence had on static torque transmission capability in steel/steel and steel/composite circular joints respectively. Sample interfaces were made polygonal to give them a partial mechanical advantage, with testing focussing on how these shapes effected torque transmission capabilities, and how different stacking sequences of the carbon fibre composite then gave the highest torque capabilities for different shapes.*

The epoxy adhesive used was IPCO 9923 and the steel was S45C. The joints comprised of either an outer and inner steel adherend, or an outer carbon fibre composite with two inner steel adherends. The polygonal shapes included triangle, tetragon, pentagon, and hexagon. Elliptical and circular were also tested.

Results from statically testing the steel/steel circular single lap joint suggested that as adhesive thickness increased beyond 0.1 mm, maximum torque decreased from a constant 190–210 MPa by 43% to 110 MPa at 1 mm. Below 0.1 mm, however, made the bonding operation difficult, and so 0.1 mm adhesive thickness was chosen for further testing. The results from the composite/steel testing are shown in Fig. 16. Results from the circular single lap joint suggested that as the stacking angle increased from ± 5° to ± 45° in intervals of ± 5°, torque capability initially increased to reach a peak at ± 25° (information shown at 30° for comparison to other studies), and then decreased as stacking angle increased. The results from the polygonal composite/steel samples are shown in Fig. 16. They suggested a decrease in torque capability for triangular and tetragonal with an increase in angle, whilst pentagonal and hexagonal showed no clear correlation over the angle change. For elliptical, maximum torque capability was found at ± 30°. This disagrees with the following study [22], which suggests 45° for elliptical. More work should be complete to gain an optimum range of layup angles.

4. Interfacial integrity

This section looks at how changing the physical properties of the interface affects its ability to retain functionality. These properties can be altered directly by changing adherend material type; thickness and stiffness; bond length; or indirectly through loading rate or temperature change. The studies below have been taken from lightweighting exercises in the aerospace/automotive sectors, and the civil engineering technique of repairing steel structures with composite patches. While the latter is not aerospace focussed, these studies offer an insight into how the interface between these materials copes after various physical changes under stress and could help advise further research.

The testing often used for these interfaces involves strap joints [30,33,34,35,36], a variation from lap joints (Fig. 9). Here, adhesion between two materials is tested by splitting one material over two bars of a different material, ensuring a gap between the two (Fig. 17). A double strap arrangement provides a more uniform shear stress within the bond layer and helps to avoid peel, commonly found on single strap joint shear testing [100]. Scarf joints can also be used, enabling the joint thickness to be maintained [101], and therefore enabling surface repairs that do not inhibit aerodynamic efficiency [96]. With the strap joints in this article, for both lap and strap testing, the force is applied to the metal in tension, creating a shear load and replicating the transmission in a hybrid driveshaft's insert to flange connection.

The typical failure mode of a join's adhesive interface, known as adhesive and cohesive failure are illustrated in Fig. 18.

The effective bond length can be described as the length in which most of the interfacial stresses are focused, maintained, and transmitted in the adhesive layer. Essentially, increasing the bond length beyond this would lead to no significant increase in load-bearing capacity. The effective bond length begins forming mainly through cracking near the applied load and shifts when the active bond zone moves to a new area further away from the loading. This debonding continues over time until the composite is completely debonded from the steel [102]. Any further increase of bond length above this threshold does not lead to an increase in bond strength [103], reported in previous studies [104,105,106,107].

Kim et al [27] studied the effect of bond length and insert, or yoke, thickness on the static torque transmission capabilities and natural bending frequency of a hybrid carbon and glass fibre epoxy composite driveshaft with circular metallic inserts, as in (Fig. 12). The study designed for torque capabilities of 3500 N·m, and for a natural frequency of 6500 RPM, as is also common for automobile studies [6,7].

The stacking sequence of the hybrid composite was $[(\pm 45)_{16,glass}/0_{carbon}]$, the inserts were 6061-T6 aluminium and the epoxy adhesive 0.2 mm thick IPCO 9923.

Torsion testing was carried out at $0.1°{\cdot}sec^{-1}$ using a shorter test sample to traditional driveshafts but with all parts included. The results for both bonding length and insert thickness are shown (Fig. 19). It was concluded that after 15 mm bonding length, torque capability begins to slow it's increase. At a bonding length of 15 mm, torque capability was 4850 N·m, higher than the required 3500 N·m. For insert thickness, it

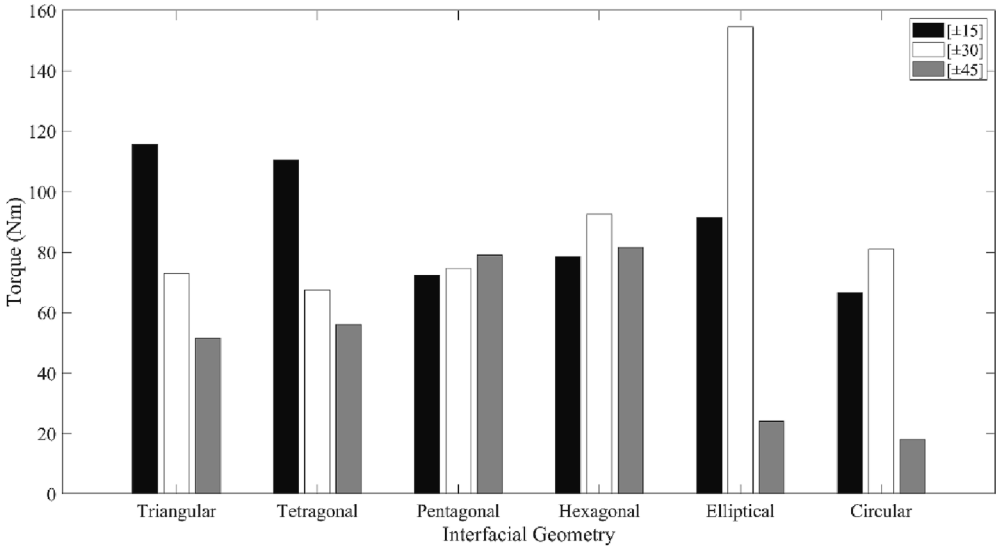

Fig. 16. Torque transmission capabilities of adhesively bonded lap joints with different interfacial geometries and composite lay-ups, . adapted from [24]

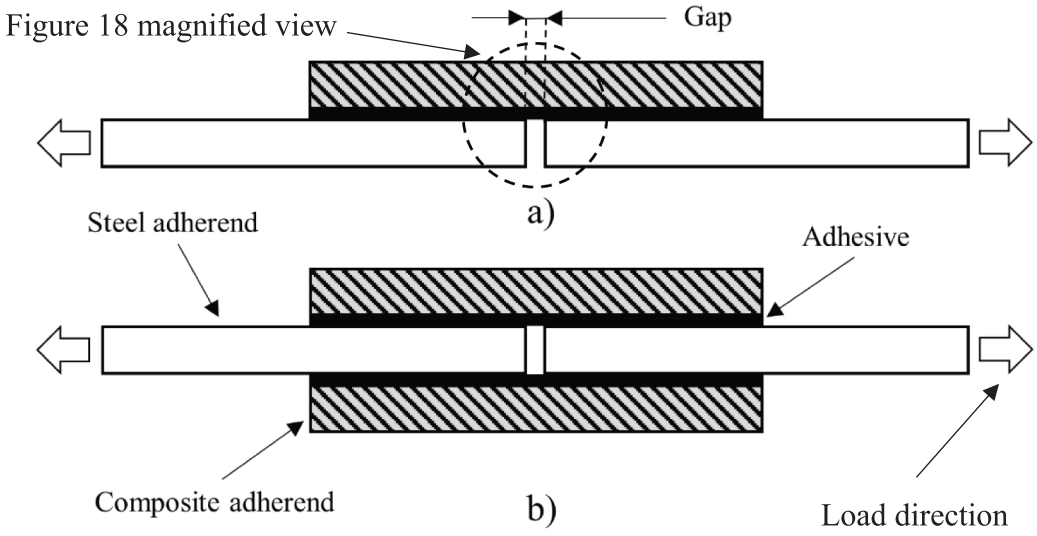

Fig. 17. Cross sections of the following: a) single strap joint b) double strap joint.

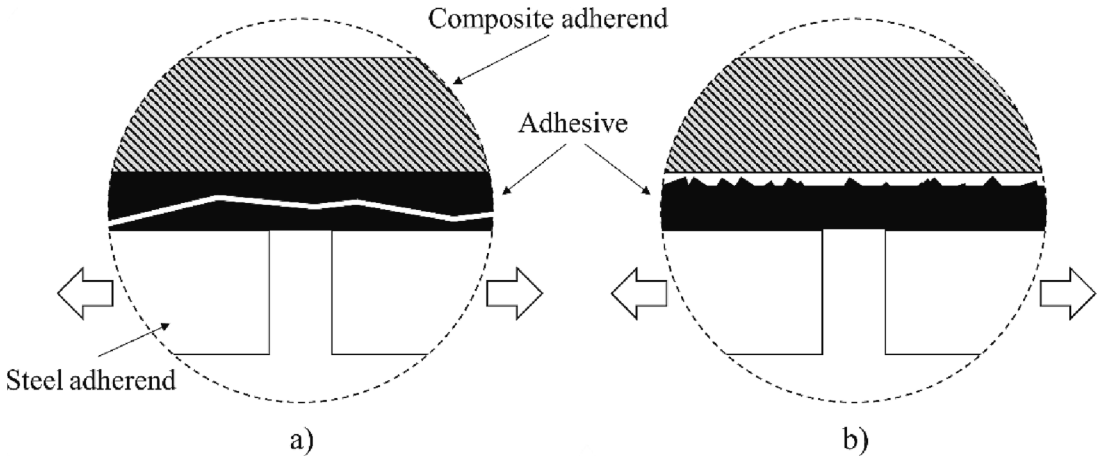

Fig. 18. Magnified single shear test showing a) cohesion failure and b) adhesive failure.

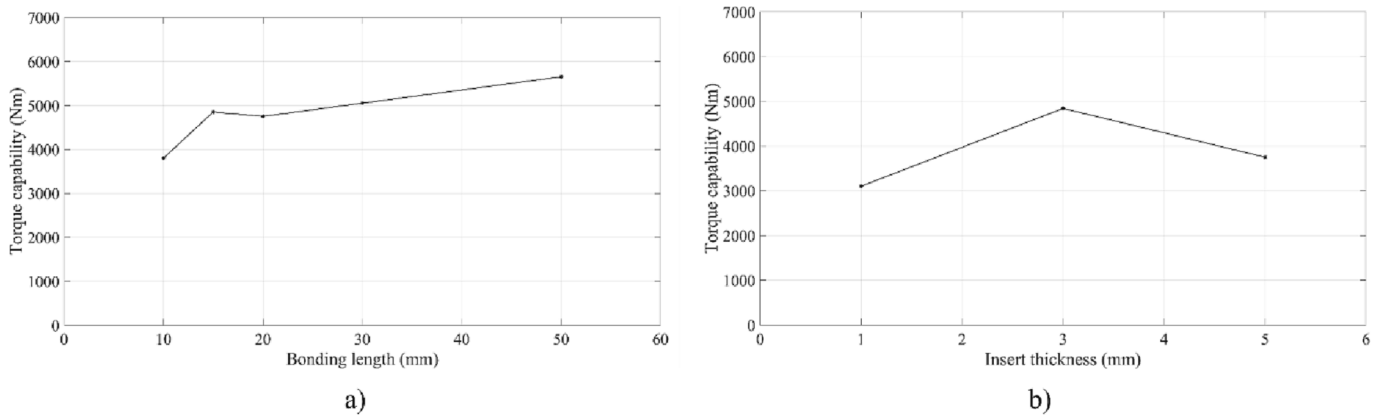

Fig. 19. Torque transmission capabilities with respect to a) bonding length and b) insert thickness, . adapted from [27]

was found that 3 mm gave the superior torque results, giving 4840 N·m. This thickness relationship can be linked loosely to [23], where a 2 mm metallic wrap around a similar composite shaft gave rise to a torque value of 4320 N·m. Furthermore, [22] gains a maximum torque capability of 4398 N·m with a 3 mm steel adherend.

Alves et al [28] reported on the effectiveness of a hybrid CFRP/

aluminium scarf joint over similar lap joints, experimentally and numerically, the former of which will be reported here, whilst also assessing effect of altering scarf angle on the joint's mechanical properties.

To ensure the study was relevant to the automotive industry's lightweight objectives, it used AW6082 T651 high strength aluminium alloy as the metallic adherend, and carbon fibre. Araldite® 2015 epoxy was used as the adherend adhesive. The composite had 20 laminae, with a ply thickness of 0.15 mm. Testing used a scarf joint of width 25 mm, at varying angles: 10°, 15°, 20°, 30° and 45°. The length between material gripping points was set to 200 mm, and the testing velocity was 1 mm·min^{-1}.

Stress analysis results (Fig. 20) concluded that the scarf joint performed well, returning only small direct stress variations along the width of the bond, comparatively fewer than similar single lap tests performed [108]. The peak direct stresses were much reduced compared to the same single lap tests, also, highlighting superior joint performance. It was suggested that this characteristic could be useful in joints with brittle adhesives that cannot withstand high peak stresses. There was, however, shear stress asymmetry apparent at either end of the bond, a characteristic explained to be due to variation in the stiffness between both materials; the higher stiffness in the composite led to peak stresses at the scarfed tip of the composite adherend. Mechanical results differed between angle when looking at both stresses, but the most significant difference occurred at the end of the bond, leading to dramatically higher peak stresses at a 45° scarf angle.

Failure was consistently found in the adhesive, with all tests ending due to cohesive failure.

Joint strength, P_m, showed reduced values for an increase in scarf angle, with strength increasing over 45° at 30°, 20°, 15° and 10° by 30.3%, 89.3%, 136.9% and 231.7% respectively, as shown in Fig. 21. The tested angles didn't manage to regain previous stress capabilities, being 32.1% lower than aluminium only, and so more angles below 10° should be tested to assess whether the join can reach or even surpass an area with a join.

Carbas et al [29] have identified that the failure of a join between CFRP and metal often occurs in the CFRP adherend itself through a process known as peeling, and so have experimentally studied the effect of adding aluminium sheets during composite manufacture in order to enhance the through-thickness mechanical properties, creating a fibre metal laminate (FML). This is a manufacturing process which has relatively limited literature [109] compared to comparable technologies, but is found in two major structural sections in the Airbus A380 commercial aircraft in the form of GLARE, a glass fibre/aramid/aluminium hybrid composite [110]. In this study, different aluminium surface treatments were tested, and an optimal joint configuration was found that gave the most resistance to peeling.

The modified CFRP used a unidirectional carbon/epoxy pre-preg of 0.15 mm thickness per ply and 16 plies in total, giving an adherend thickness of 3.2 mm. The metallic adherend was 2024 – T3 aluminium

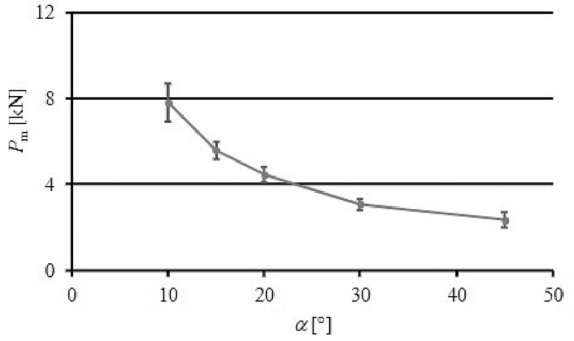

Fig. 21. Maximum load in joint against scarf angle, taken from [28].

alloy, and the study compared both 0.8 mm and 0.4 mm adherend thickness. To retain the overall material's 3:1 by volume ratio of CFRP to aluminium respectively, one 0.8 mm and two 0.4 mm aluminium sheets were used. Single lap joints were created, with 95 mm length and 3.2 mm width adherend plates, 0.2 mm adhesive thickness, and a bonding overlap of both 12.5 mm and 50 mm. Tensile testing occurred at 1 mm·min^{-1}.

The main results from tensile testing showed that the addition of aluminium plating reduced instances of delamination leading to failure, and instead more cohesive failure. The method can therefore be recommended for reducing peel failure (peel stresses are a major source of delamination). Whilst this method was also found to increase weight by 15.6%, this decrease in peel strength at the overlap may be critical to certain applications, irrespective of weight increase. The ultimate hybrid lay-up was found when the aluminium layers were external, giving rise to the highest joint strength (Fig. 22). FEA analysis developed as a part of this study, using ABAQUS®, aligned well with the joint

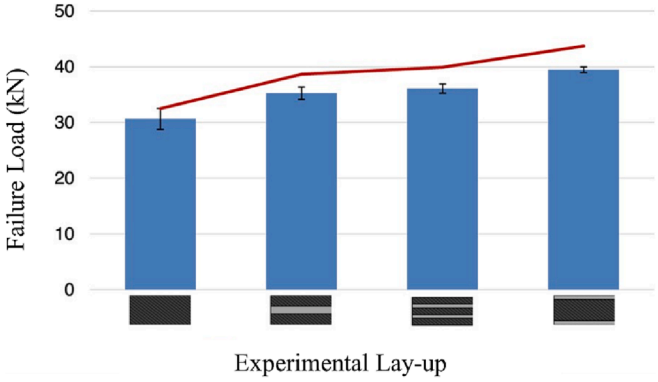

Fig. 22. Failure loads with a 50 mm overlap (experimental and FEA predictions), taken from [29].

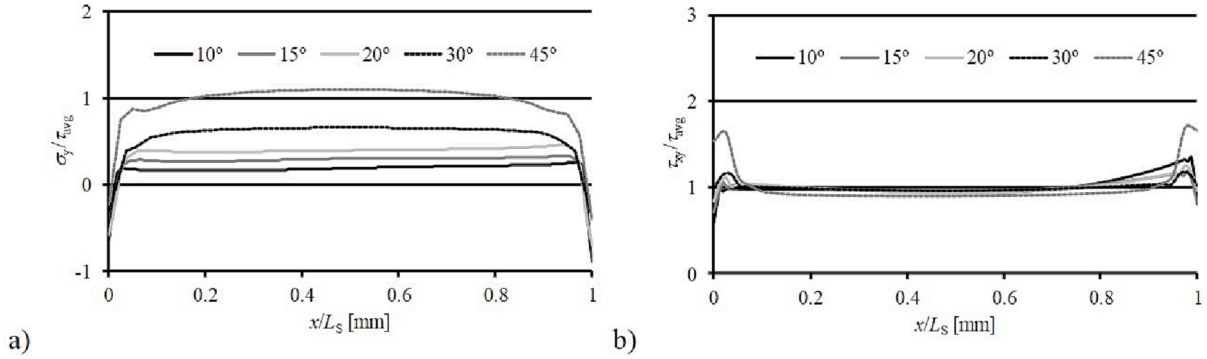

Fig. 20. A) Direct and b) shear stresses for mid-thickness scarf joints at varying angles, taken from [28].

strength obtained experimentally.

Surface treatment experiments concluded that Phosphoric acid anodizing was the best surface treatment, compared with no treatment and sandblasting. Adhesion between dis-similar adherends was better than between like adherends. Furthermore, there was found to be high residual thermal stress in the hybrid joints, primarily due to the mismatch in CTE.

Further work on FML's can be found mostly in the aerospace sector, with examples including ARRALL (aramid-fibre-reinforced aluminium composite) and CARRALL (carbon-fibre-reinforced aluminium laminate) [111]. Early work here includes looking at thermal residual stresses from curing [112] in single-lap joints between CFRP/aluminium FML's. Results concluded that whilst there was considerable geometry change after curing, the FML joint strength was more than 35% higher than composite-only lap tests. Furthermore, when comparing aluminium layer positioning, it was found that, unlike in [29], performance in samples with just one metallic layer equalled those with two. This naturally leads to a higher specific strength, and should be studied further for the benefit of weight-saving in aerospace applications.

Jimenez-Vicaria J et al [30] focussed on the effect that individual carbon fibre stiffness and adhesive ductility had on steel/CFRP bonding under tension, and how bond length effected the failure mode. Here, shorter bond lengths of 30 mm and 60 mm were studied compared to the 300 mm bond lengths found in previous literature of 300 mm [106,113].

The testing setup involved preparing double-strap joints, where grit blasted S275 JR steel plates were aligned and separated by 2 mm to replicate in-service steel fracture, as in Fig. 17. Epoxy adhesive was applied and a single CFRP plate of thickness 1.8 mm and width 25 mm was set perpendicular across the joint and compressed until the desired adhesive thickness of 0.5 mm was reached. During tensile testing, a displacement control of 0.5 mm•min^{-1} was used, with strain gauges attached for analysis.

Firstly, it was concluded that for longer bond lengths of 60 mm, it was better to use a ductile adhesive (2.98% failure strain) and a stiff fibre (183,605 MPa tensile modulus), with experimental joint strength peaking at 63,630 N. However, the opposite was found for shorter 30 mm bond lengths, where the highest strengths were obtained with a brittle adhesive and a less stiff fibre with joint strength peaking at 42,180 N.

Failure mode was determined to be dependent on bond length rather than type of carbon fibre or adhesive. Shorter bond lengths of 30 mm led to a failure mode that was consistently produced by adhesive layer separation at the steel surface. For 60 mm, adhesive failure for both the steel and CFRP, interfaces occurred, as well as cohesive failure.

Finally, using strain gauges along the centre line of the CFRP plates during testing, the stress distributions of the different sample combinations (bond length, adhesive and CFRP type) were identified. The stress was calculated by multiplying the measured strains with the modulus of elasticity of the carbon fibre composite. The results suggest that that stress did not change considerably with changing adhesives, but an increase in CFRP stiffness saw the peak increase from approximately 440 MPa to 570 MPa in the 60 mm samples and a peak increase from approximately 220 MPa to 250 MPa for the 30 mm sample.

Amraei et al [31] studied the feasibility of using high and ultra-high strength steel (HSS/UHSS) when strengthening civil structures using CFRP. The bond between the steels and the CFRP was assessed, using single and double-sided bonding to assess debonding load, failure mode and maximum overall stress. The results here are useful for aerospace and automotive industries, where higher strength steel usage is common [114], as opposed to mild steel, which is currently the focus of most civil studies.

Three steel types were used: S700, S960 and S1100, in conjunction with ultra-high modulus (UHM) CFRP. Both materials were manufactured into plates, using 0.4 mm thick Araldite® 420 A/B epoxy as the bonding adhesive. Quasi-isotropic tensile testing at a displacement control of $4 \times 10^{-5}s^{-1}$ was used, employing DIC similar to Fig. 26 to measure strain values on the plates.

Results suggested firstly that the double-sided bonding didn't allow debonding to occur as in the single-sided test, instead fully employing the CFRP plate, leading to steel rupture outside of the CFRP strengthened region. The debonding in the single-sided test was as a result of a combination of steel-adhesive interface failure, cohesive failure and adhesive-CFRP interface failure. When comparing to mild steel, the HSS and UHSS with higher yield strengths led to higher debonding loads also, increasing the efficiency of the overall join. For example, compared with S700 mild steel, HSS increased maximum bond load by 29.4% to 29.6%, and UHSS by 29.8–30.3%. This debonding load for Araldite® 420 when utilised for bonding the two materials was six-times higher than the adhesive's shear strength. Furthermore, single and double CFRP sided specimens reduced stress in the steel by 18% to 24% and 43% to 45% respectively.

Amongst very limited studies, **Jiao et al** [115] also looked at very high strength steel and its interaction with bonded CFRP strengthening. Here, circular butt-welded tubes were strengthened with fiver layer CFRP and Araldite® 420, and were double strap shear tested. Again, good performance results were obtained, with the CFRP join increasing strength up to 200% over welding alone. An effective bond length of 75 mm was found, around twice the diameter of the tube.

Al-Mosawe et al. [32] investigated how the bond between CFRP laminate and mild steel plate in double lap joints are affected by increasing loading rates. A comparison was made by testing at 2 mm•min^{-1} quasi-static loading, and 201×10^3 mm·min^{-1}, 258×10^3 mm·min^{-1} and 300×10^3 mm·min^{-1} for dynamic loading, so-called due to their comparatively high loading rates; Hydraulics were used for the quasi-static tests, and a drop-mass rig was used to gain the differing dynamic loads. Ultimate joint capacity and effective bond length were the main outcomes when comparing the strain rates in this study, whilst also comparing low (159.4 GPa), normal (203.0 GPa), and ultra-high modulus CFRP, the latter of which was from another study in literature. The testing was stopped either once failure occurred in the samples, or once the drop had been completed. often once the joint capacity levelled off. The bond lengths used for quasi-static and dynamic tests were 30 mm to 130 mm and 30 mm to 110 mm, respectively.

When analysing results, the three dynamic loading rates showed similar results, suggesting a weak link between differing load rates and differing outcomes, but a strong link when comparing static and dynamic loads in general. The results showed that the maximum joint capacity increased 48% from dynamic testing, for example there was an increase from 51.7 N to 107.1 N for normal modulus CFRP laminate. Also, there was a lower effective bond length associated with dynamic compared with static: 90 mm and 110 mm respectively. This improvement after an increase in loading rate was attributed to the high shear strength of the adhesive under high loading rates. The effective bond length for high loading rates was found to be less than for quasi-static loading. Ultimate strain, however, was found to be unaffected by a higher loading rate. When looking at failure modes, it was mostly found in the adhesive layer, or cohesive failure (Fig. 18), suggesting that the adhesive made the biggest contribution to load bearing. This aligns with [30], where cohesive failure only occurred in the higher bond lengths of 60 mm, suggesting cohesive failure may occur more often in higher bond lengths. A comparison with UHM CFRP in literature [116] gave the conclusion also that bond stress in normal modulus CFRP was higher than with UHM CFRP, explained to be due to a higher tensile strength and ultimate strain of the normal modulus CFRP, leading to less adhesive stretch and ultimate delamination.

Al-Shawaf et al.[33,34] focussed on the effects that sub-zero temperatures have on the bond behaviour of *retro*-fitted CFRP laminates on mild steel. Here, testing on a double-strap joint was chosen to best replicate this in-service by focusing on shear loads and to minimise adhesive peeling, as in Fig. 17.

Each CFRP laminate was made up of 3 plies of unidirectional carbon fibre composite sheets. Al-**Shawaf et al** [33] used a single epoxy

adhesive, Araldite® 420 A/B, and in [34] used three versions of CFRP with different matrices including Araldite® 420 A/B, MBrace® Saturant and Sikadur®.

Specimens were tested at 2 mm·min^{-1} displacement control to failure, at four different temperatures: −40 °C, −20 °C, 0 °C and 20 °C, using a soak time of 10 min [33] to one hour [34].

The most common type of failure mode was cohesive failure in the adhesive layer, which in these studies, as opposed to [30,32], resulted in interfacial debonding. There were minor incidents of CFRP fibre tear which may have indicated good steel surface preparation. Araldite® and Sikadur® epoxies showed negligible bond strength difference after exposure to sub-zero temperatures compared with ambient, although the MBrace® Saturant samples revealed a 40% decrease in bond strength after exposure to −40 °C.

Nguyen TC et al [35] looked at how the mechanical performance of a double strap joint of CFRP/steel is affected by elevated temperatures of between 20 and 60 °C. It again highlighted the use of this technique on the retrofitting of composite plates onto an ageing steel structure. The importance of this stems not from the worry about the carbon fibres themselves, which are able to withstand very high temperatures (less than2400 °C)[117], but from the matrix, where temperatures higher than the glass transition temperature could lead to FRP failure. Aerospace-grade thermoset epoxies often have a glass transition temperature of between approximately 40 °C [36] to 150 °C [118]. Furthermore, traditional thermoplastic matrices such as (PEEK) can reach up to 140 °C [119], and [120,121] suggest that a new generation of thermoplastic polymers such as polyaryletherketone and thermoplastic polyimide could increase this to 250 °C. The adhesive layer is also of concern, with a study suggesting only 22% of the initial strength of a CFRP/Steel double strap joint is retained when heated above 60 °C [122].

The study used Araldite® 420 adhesive with a glass transition temperature (T_g) of 42 °C. It was shown that with an increase in temperature from 20 °C to 50 °C, effective bond length increased from 40 to 100 mm for single lamina CFRP sheets, and similar results followed for triple lamina CFRP sheets. Stiffness then decreased considerably with an increase in temperature, where a 20% reduction was seen at T_g, 50% at 10 °C above T_g, and 80% at 20 °C above the T_g. Strength saw a similar drop, with ultimate tensile strength at 40 °C and 50 °C decreasing 10% to 15% and 50% respectively.

The failure modes were examined at the different temperatures. At lower temperatures, the joint failed through CFRP delamination. As temperatures increased to and went above the T_g, failure became cohesive due to the dramatic reduction in mechanical properties of the adhesive at these temperatures.

Liu HB et al [36] looked at the effect of short-term elevated temperatures on the characteristics of the bond between wet lay-upped CFRP sheet and steel, and the influence of multiple layers. It examined strain distribution along the bond length, ultimate strength, failure modes and effective bond length.

The reinforcements were Mbrace® CF 530 high modulus carbon fibre composite sheets, each having a thickness of 0.19 mm, and the adhesive used was Araldite® 420.

The testing used double strap joints, which were tested at three temperatures 20 °C, 40 °C and 50 °C, representing room temperature, glass transition temperature and above respectively. Bond lengths were varied from 10 mm to 120 mm. Tensile tests were performed at 2 mm·min^{-1}.

The joint with one layer had a much higher strain at each temperature than those with three layers, explained to be because of shared strains over a larger thickness. Strain in the joint for both thicknesses decreased slightly from 20 °C to 40 °C as bond strength decreased 10%, and significantly from 40 °C to 50 °C as bond strength decreased 40%.

Across all temperatures and thicknesses, joint failure occurred through fibre breakage and cohesive failure, with fibre rupture occurring at the joint. This was contrasted to **Nguyen et al** [35] in which a similar setup but with normal modulus CFRP was used. Differences were explained to be due to the epoxy having a tensile strain lower than the carbon fibres, meaning the strain limitation was defined by the matrix, leading to matrix type failure. For high modulus CFRP, the strain limitations were defined by the strain of the fibres, leading to fibre type failure.

SEM inspection found that with increasing temperature came larger air pockets within the matrix, likely reducing the strength of the composite. The initial smaller air bubbles are often a defect of manufacture for CFRP, where air entrapment can occur during the impregnation and consolidation stages, or as a result of poor filament wetting [123]. The negative impact from the air pockets on delamination in composites, and hence strength seen in this study, is also found similarly in the following [124,125,126,127].

Finally, the bond test showed that high modulus CFRP sheets of any thickness generally have longer effective bond lengths at each temperature, and one sheet joints showed longer effective bond lengths than three sheet joints.

5. Corrosion and moisture absorption

When determining the efficacy of hybrid driveshafts in real world conditions, such as auxiliary or main driveshafts in gas turbine engines, automobile or marine transmission shafts, the corrosion of the connecting metallic and how this will affect the overall performance must be fully understood. This section, therefore, highlights the ways in which corrosion may affect the bond between a metallic and a composite.

This corrosion work is still in its infancy with regards to driveshafts, particularly in the aerospace sector, partly due to on-going studies questioning an FRP's ability to cope in water-rich environments [128,129,130,131,132]. Here, the moisture has been found to diffuse into the epoxies and adhesives, leading to hydrolysis, causing chain scission leading to a decreased polymer crosslink density [133]. This in turn leads to matrix plasticisation, micro-cracking, and voids. These in turn have been proven above to reduce the mechanical properties of the material, whilst also allowing corrosive liquid into metallic regions of the driveshafts. These findings along with high temperature exposure, where plasticisation reduces a materials T_g [134], have led to few FRP composites used in service critical regions of gas turbine engines where water may be more common, and instead are being used as, for example, axial driveshafts [90], slowing the research on the effects of corrosion of these parts over time. This then has led to the addition of civil engineering studies in this section [37], which looked at the retrofitting of pre corroded metal with CFRP, bringing positives of higher load bearing capacities and durability, whilst lowering stress concentrations. This does, however, come with a corresponding debonding found after repair. This information is useful still for aerospace applications, which would benefit from the mechanical advantages, and where water exposure over time may lead to this corroded surface post installation and progress to similar failure.

One of the corrosion types that could be encountered includes galvanic, commonly found at a junction between two materials in areas of high saltwater content. Here, the cathodic CFRP has been shown to provide the electrochemical difference required for this type of corrosion to occur between it and steel, reducing the service life for an adhesive bond between these two materials [135,136]. This interaction isn't limited to steel either, and the significant use of aluminium in hybrid driveshafts [10,17,23,27] will be subject to this type of corrosion too [137,138]. Whilst an epoxy content of the CFRP is understood to reduce this effect, just 1% breaks in an epoxy has been shown to lead to an unacceptable steel loss of 0.018 mm per year [139]. A possible solution to this could be the use of more glass fibre reinforced polymers (GFRPs) in high salt areas, or as in [3,17], to add glass fibres into a carbon fibre composite material.

The authors have studied the effect of salt corrosion on the interfacial

strength between steel and CFRP cross sectional samples with a microspline interface, as in Fig. 8. The testing utilised a novel, modified 'push-out' test. This method is usually either used to test the interfacial properties of individual fibres in a fibre reinforced composite [140], or in civil engineering where the bond behaviour between a circular steel/composite structure can be examined [141]. It was used here as an alternative to larger scale torsional testing, as the availability of such testing is often limited due to high cost.

The 2 mm width samples were cut from the ends of an aerospace-grade driveshaft, where carbon fibre with BMI resin wrapped around steel inserts, used for connecting the composite shaft to an applied torque. Only two samples at each exposure time were tested to gain an average due to limited material supply. Some of these were then exposed to 3.5% salt spray, 99.5% pure sodium chloride at 70 °C for varying times up to 1008 h, according to ISO 9227. To allow for a comparison, other samples were not exposed and were push-out tested beforehand.

The testing involved placing the cross-sectional samples within an indented steel plate, which had a diameter just larger than the outer diameter of the sample, to hold it in place. A disc for each sample, manufactured the same depth as the sample and with a diameter the same as the inner diameter of the steel, was placed inside the sample. This had a lip on the upper surface with a larger diameter, large enough to cover most of the steel in the sample, without overlapping the interface. This insert was then pushed from above, applying equal pressure on the steel without relying on exact alignment (Fig. 23).

This push-out testing ran at a displacement controlled 0.2 mm • min^{-1}. Fig. 24 shows the full 5 mm normalised results, comparing virgin through to 1008 h. The results suggest there is a general increase in load from virgin to 1008 h of around 42.3%. It also suggests the following: 96 h of corrosion had little effect on load, with just a 6.7% decrease, and past this, there is little correlation between corrosion time and load increase, other than the overall increase (circled), with the percentage load increase varying between 26.1% and 46.5% over virgin. This initial increase in strength may be a result of oxidation expansion, found also in [142,143] in civil applications, where the corrosion products increase the radial pressure on surrounding materials at their interfaces, potentially leading to further damage in these other materials.

This method is still in its infancy, and further testing alterations should be established to fully understand the link between salt corrosion exposure time and the change in interfacial strength. Such improvements could include: increasing the sample size for all sample conditions, fully exploring a link between sample distance from shaft edge and maximum load, and exposing for longer than 1008 h to find a point at which load decreases beyond the initial virgin state. This latter improvement would hope to find the point at which the oxidation expansion phenomenon is overcome by the loss of interfacial contact surface area of the join, found in [144,145], resulting in lower static friction.

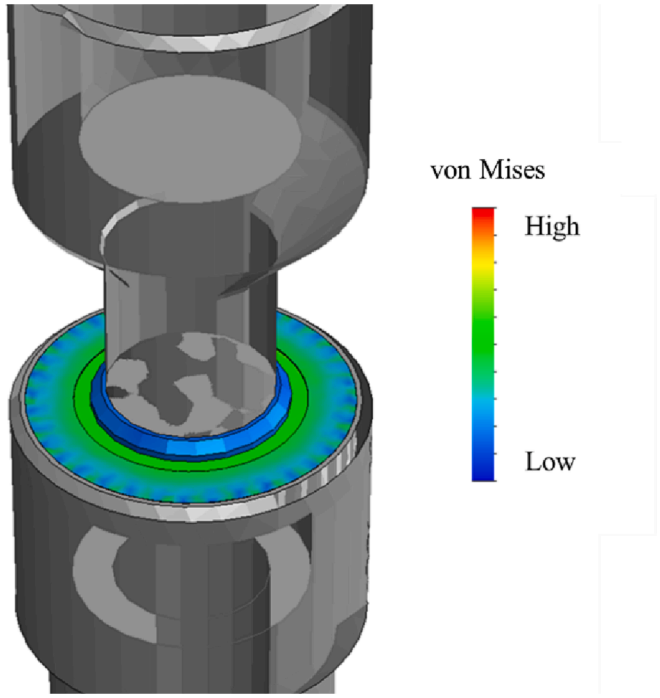

Fig. 23. Push-out model showing stress mapping across 5 mm sample.

Shanhua Xu et al. [37] looked at the effect of corrosion on the bond in CFRP reinforced steel joints by single lap shear testing, focussing on failure modes, load–displacement effects and shear stress.

The steel used in this study, cut from steel plant U channels, had been pre corroded for 10 years, and was subject to high humidity and temperatures from nearby aggressive gases, with concentrations of SO_4^{2-} and NO_3^-. Samples of five different corrosion levels were taken, ranging from no corrosion to multi-layered corrosion. The adhesive was two-part epoxy, and the CFRP was unidirectional with a 1.4 mm thickness.

Typically, adhesive failure usually occurs at the adhesive/steel interface, rather than the interface with CFRP [146], therefore the steel surface is the focus of investigation. Quantification of steel corrosion was done using equation (9) to define mass loss ratio, ξ:

$$\xi = \frac{W - W_0}{W_0} \times 100 \tag{9}$$

where W_0 and W are the weight before and after corrosion, respectively. Here, the weight loss ratio ranged from 12.48% to 28.74% for scattered corrosion pits and multi-layered corrosion respectively. The irregularity of the corrosion was in part due to the pitting of various sizes seen in the corroded steel. This was evaluated by taking six profiles along the loading direction at the loaded end, where pit width was defined as the distance between the two maximum points, and pit height was defined as the difference between the trough and the larger maximum point (Fig. 25).

The CFRP/steel specimens were created with single lap joints to simplify the inspection with only one path for debonding. The bond length was 240 mm, situated between a 700 mm length CFRP plate and a 240 mm length steel plate. The curing of the adhesive took 2 weeks at room temperature in this state.

The shear test (Fig. 26) involved bolting the specimen to a base to inhibit movement and attaching a hydraulic jack to the CFRP plate. The jack would load at 500 N increments during the linear phase and 250 N in the nonlinear phase. Strain gauges were also attached to the CFRP. DIC technology was used to measure relative displacement between CFRP and steel plate at the loaded end.

After testing, only the failure mode near the loaded end was studied, as further away from the loaded end, the failure occurred because of the bonded ends failure, not as a direct result of shear. In general, it was found that as levels of corrosion increased in the samples, failure changed from adhesive failure to cohesive failure. Firstly, on the samples with low corrosion (pitting only), adhesive failure dominated due to the smaller contact surface area, resulting in a weaker interface. It is important to note here that that pitting had little effect on outcome when compared to zero corrosion. With the presence of more corrosion, the main failure mode was still adhesive between steel and adhesive. This was explained to be because of excessive aspect ratio, and the large surface area would have caused an uneven adhesive layer, increasing the likelihood of the adhesive peeling off. In the two samples with the highest level of corrosion, whilst the aspect ratio was still high, the standard deviation was lower, resulting in sufficient mechanical interlocking. This then led to a steel/adhesive interface that had a higher strength than the adhesive layer, leading to cohesive failure. It is then concluded that extreme values of aspect ratio and standard deviation lead to the interface weakening.

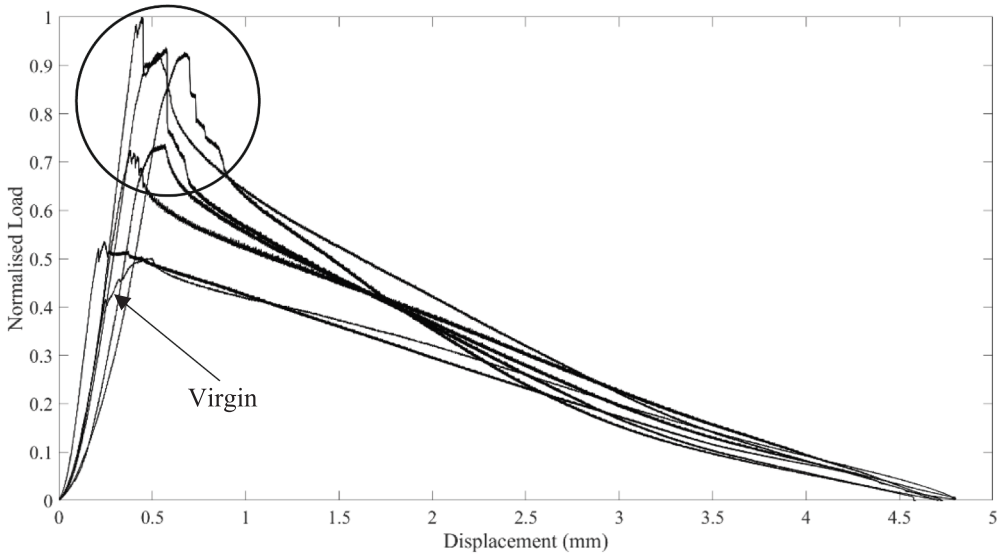

Fig. 24. A graph comparing the normalised load for virgin and exposed cross-sectional samples after push-out testing.

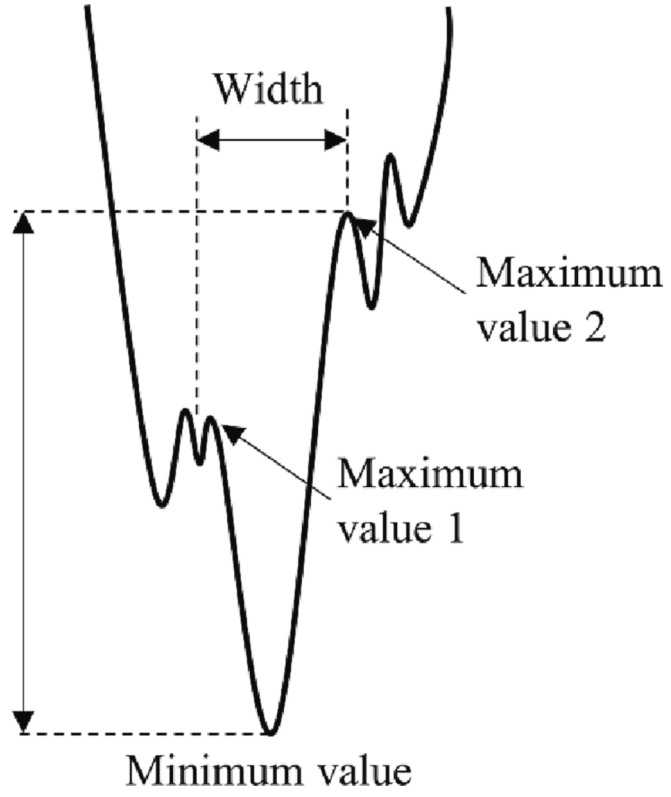

Fig. 25. Corrosion pit identification, .
adapted from [37]

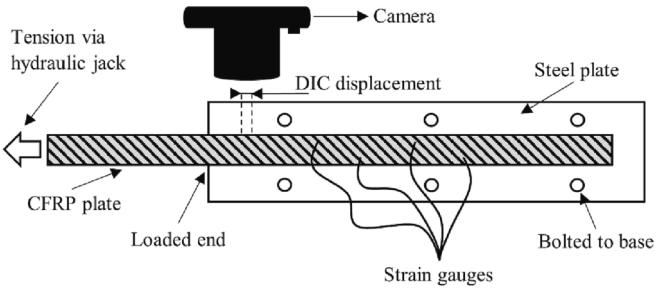

Fig. 26. Top-down single lap test, .
adapted from [37]

When looking at the load–displacement effects of corrosion, the behaviour can split into an elastic stage, an adhesive softening stage near ultimate load and finally sudden failure. The first four samples up to dense pitting showed this sudden failure, indicating a steel/adhesive failure. However, for corrosion above this there existed a long plateau in the failure stage, suggesting the adhesive held bonded long enough to show the samples ductility. (Fig. 27) shows the difference between zero (a) and high, multi-layered (b) corrosion respectively.

The improvements continue when looking at average ultimate load, with the most corroded samples of greater than 15% outperforming others significantly (Fig. 28). This effect was compared to other studies by **Teng et al** [146], where increasing the fractal dimension of the steel surface led to an increase then levelling off of the ultimate load. This was attributed to the blasting not being enough to lead to adhesive peeling.

Corrosion led to a more immediate decline in shear stress after the loaded end, attributed to the irregular surface converting the interfacial stresses from steel/adhesive shear to composite, interfering with the stress distribution along the bond area. The effective bond length was seen to decrease with increasing pit aspect ratio, indicating that sharper corrosion pits can improve load transfer efficiency.

Ocaña et al [38] compared two adhesives and their bonds, commonly used in composite/metallic joins in automotive applications such as driveshafts and chassis. The comparisons were made after exposure to ‘adverse operating conditions’, including prolonged environmental exposure and high temperature immersion in engine oil.

The samples consisted of bulk adhesive tensile specimens, using both Loctite® 9466 epoxy and Teromix® 6700 Polyurethane. Furthermore, adhesive joint specimens were fabricated using a five-layer carbon fibre as the composite, with high-performance 6 K fibre tows and Resoltech® 1050/1056 epoxy resin. The metallic adherend was 6160 aluminium alloy. Pre-exposure was split into environmental and thermal/moisture degradation. Environmental exposure involved leaving all samples in city air over a period of up to 12 months, with high concentrations of SO_2 and NO_2, large temperature variations and significant rainfall. Thermal/moisture exposure involved all samples placed in an 80 °C climatic chamber whilst immersed in Castrol 10 W-50, 4 T motor oil for up to 128 h.

The bulk adhesive samples were tensile tested, and the joints used an

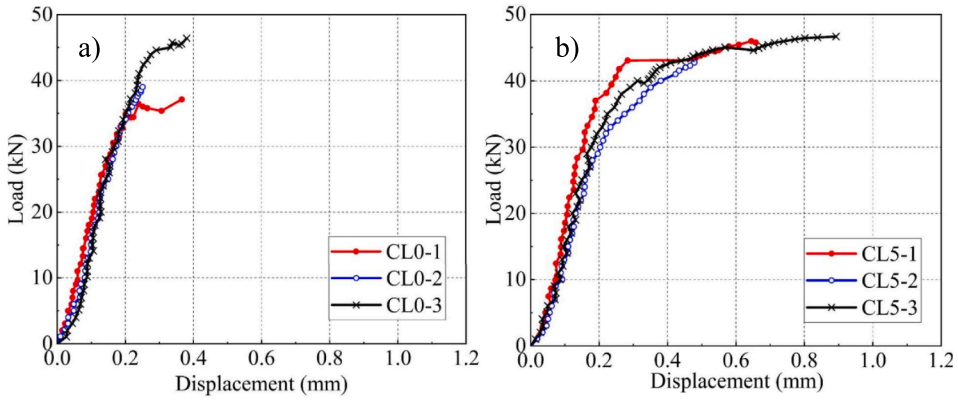

Fig. 27. Load-displacement curves for a) zero corrosion samples and b) high, multi-layered corrosion, . adapted from [37]

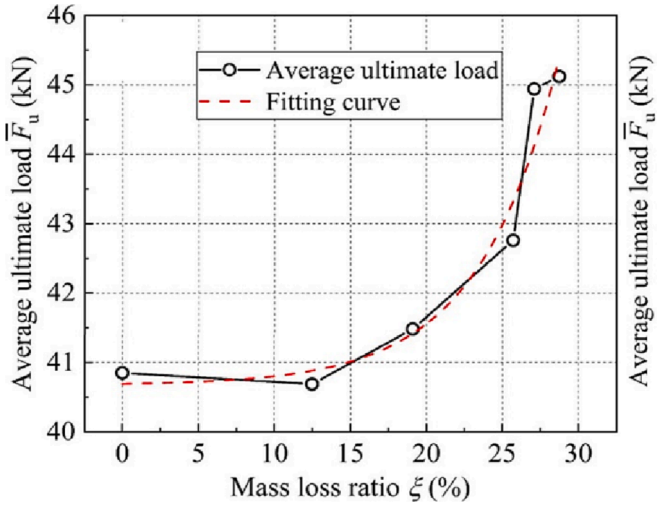

Fig. 28. Average ultimate load against mass loss ratio, or more generally corrosion severity [37].

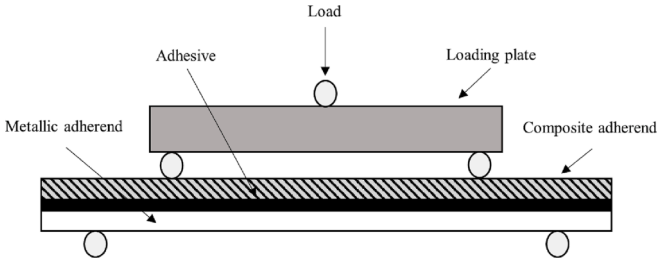

Fig. 29. ENF testing schematic, . adapted from [147]

End Notched Flexure (ENF) test (Fig. 29), commonly used for metallic and polymer composite adherends [147]. Rates of 1 and 2 mm·min^{-1} were used for the tensile and ENF testing respectively.

Post environmental exposure showed that the ENF bending strength of the epoxy joints decreased by 3.5% in shear strength after the full 12 months to 1.07 MPa. Polyurethane joints showed an 11.8% reduced strength, and overall, performed worse by approximately 50%, with a shear strength after 12 months of approximately 0.51 MPa. The tensile testing of the bulk adhesives suggested similar trends, but instead showed a 3.5% increase in strength after 12 months to approximately 42.5 MPa, however with a clear negative trend that may have led to lower values over a longer period. This was compared again to Polyurethane which decreased by 10.5% after 12 months to approximately 16.5 MPa, performing worse again by over 60%. To note, all tests showed an initial increase after a few months, which was explained to be due to the post-curing effect from the elevated summer temperatures and humidity.

Post high temperature oil immersion ENF results show a slight shear strength increase for the epoxy joints of 1% after 128 h to approximately 1.2 MPa. This contrasts with Polyurethane which had a reduced shear strength of approximately 50% to approximately 0.3 MPa. The results from the bulk adhesive tensile testing shows that there was no change in the epoxy sample after 128 h, remaining at approximately 40.5 MPa. The Polyurethane, however, increased by 35% to approximately 25 MPa. Again, the post curing effect seen in the environmental exposure samples was also found in the early hours of immersion.

Oudad et al [39] looked at the effect of humidity and the corresponding absorption on adhesive-only mechanical properties, focussing on understanding the behaviour of adhesives often found in composite repairs on aluminium aircraft structures.

The samples consisted of 4 mm thick Adeckit A140 bulk epoxy adhesive only, and were aged by immersing in distilled water at 30 °C. Water mass absorbed was determined by weighing the samples before, M_o, and after immersion, M_t. Water was absorbed into the adhesive at 0.5% for 5 days and 2% after 30 days, using equation (8). Tensile testing was conducted after immersion on sixty dog bone samples at 0.3 mm·min^{-1}.

The results suggested a strong correlation between water absorption and a drop in mechanical resistance of the adhesive, shown in the following stress–strain graph (Fig. 30). Here, there was a 58% reduction in tensile strength after 15 days, after which it remained constant as the adhesive reached saturation. Plastic strain showed variation after 10 days with an 18% increase, going to 25% after 30 days, suggesting a decrease in strength and an increase in ductility due to the plasticising effect of water, making the polymer chains more mobile, and potentially durability with increased immersion time.

6. Coefficient of thermal expansion

Studies presented in this review up until now have focussed on the effect that elevated temperature has on a CFRP/metallic adhesive interface, these have been close to the glass transition temperature, and therefore do not look specifically at the coefficient of thermal expansion (CTE) discrepancy between the two materials. Potential issues could arise from the differences in CTE between a metallic end fixing and the composite mid-section. For example, steel can have a CTE six times greater and aluminium 10 times greater than a typical carbon/epoxy

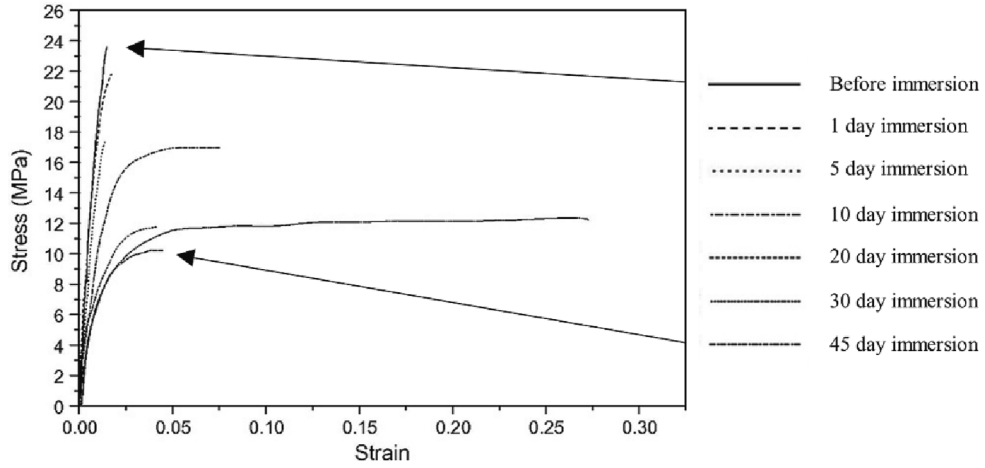

Fig. 30. Stress–strain graph at different immersion times, .
adapted from [39]

laminate [148]. Composites have quasi-isotropic CTE properties when they have equal laminae layers at 0 and 90°. Some aramid and carbon fibres can also often exhibit a negative CTE in their axial directions, but will always be positive in their transverse directions, whilst also being of a much higher magnitude than the axial expansion. This is because the matrix has a higher constraint in the axial direction than in the transverse, allowing more movement in this direction. Whilst the axial CTE in quasi-isotropic composites with carbon fibres are often higher than unidirectional, it is still very small, and is often possible to reduce this to near zero. However, transverse CTE for these quasi-isotropic composites can still be relatively large [1].

This mismatch can be especially pressing for future driveshaft components that may have a desired use in high temperature environments, such as gas turbine engines. Furthermore, when specifically exploring applications in gas turbines the reduction in temperature with increased altitude creates a freeze–thaw cycle, making it important to look at the current knowledge related to this in civil engineering.

The authors have studied the effect of CTE discrepancy on an auxiliary radial driveshaft that employs a hybrid system of steel metallic inserts in a BMI-resin CFRP shaft section. Similar to Fig. 8, the insert had serrated microsplines around its outer diameter, which during manufacture was pushed into the composite cross section. This method did not require adhesive, and instead slid through the composite using a lubricant, relying on the interference fit of the high surface area spline surface to hold it in place. This method omitted the need to account for adhesive CTE in calculations, but led to more potential issues after temperature exposure, as the integrity of the join between the materials relied solely on the correct surface contact between steel and composite.

Theoretical calculations were carried out before testing, using approximated CTE values of other similar materials. This presents a predicted interfacial gap, over a range of temperatures, of a circular join between steel and composite (Fig. 31). It shows two equal composites, S02 and S04, both with $[45/-45/0/90]_S$ but with S02 having 16 plies and S04 having 32. Fig. 31 suggests that at temperatures of 100 °C, 200 °C and 250 °C, the interfacial gap at temperature between the steel and the 32-ply composite would be 10 μm, 21 μm and 31 μm respectively.

The degree to which this interfacial gap opened or widened at these different temperatures was also experimentally investigated. Samples were exposed for 20 h, at three temperatures between 100 °C and 250 °C, which closely represented expected service temperature, operating temperature and a condition that would likely show an extreme response, respectively.

As expected, samples at 100 °C showed no signs of permanent

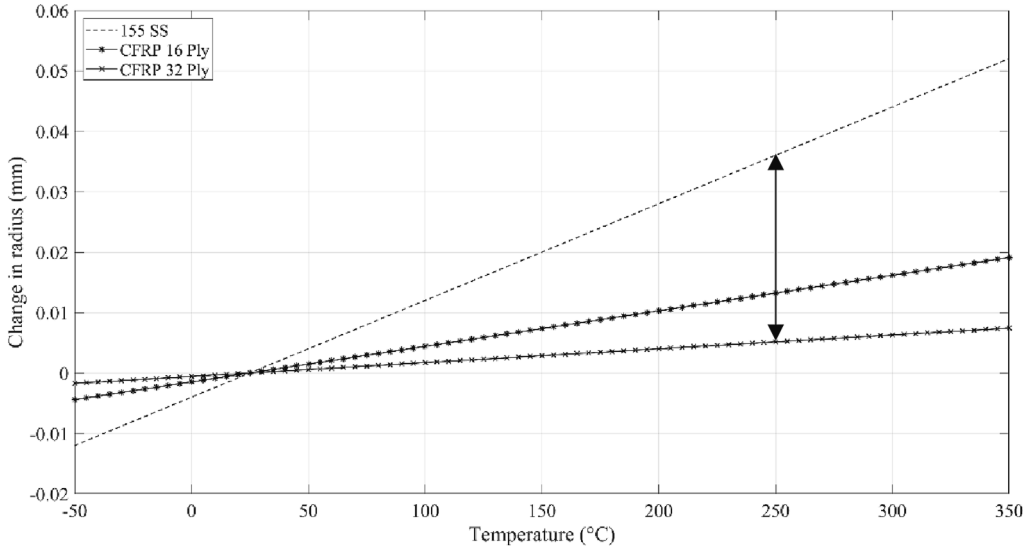

Fig. 31. CTE gap between steel and CFRP, .
adapted from [149]

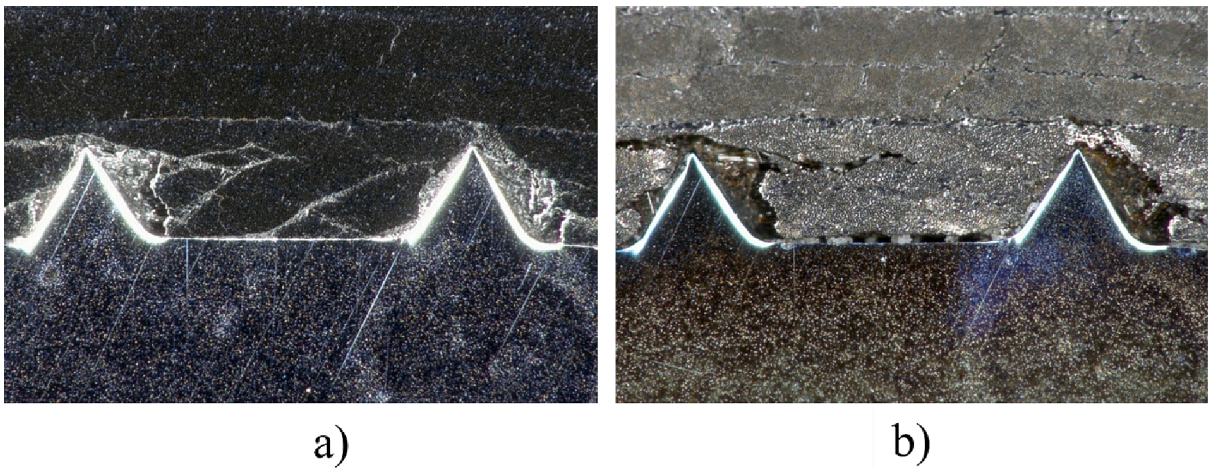

Fig. 32. Optical microscopy of interface a) before exposure b) after extreme exposure condition with interfacial gap.

interfacial opening, with the same outcome was found at the operating temperature exposure. At 250 °C, a close-to-theoretical average interfacial gap was seen to open along the whole length of the interface shown (Fig. 32). This gap not only reduced the interfacial surface area, potentially reducing the shafts torque capabilities, but could also exacerbate any corrosion between the two materials by providing a route for salt water. This highlights the importance of understanding any CTE mismatch between materials and the proposed operating conditions. Likewise, further mechanical testing is recommended here to assess the potential decrease in mechanical performance.

Wang et al [40] investigated the effect of temperature cycles from −20 °C to 40 °C on CFRP plate, bulk adhesive specimens and CFRP/steel bonds, looking specifically at CTE discrepancy between the materials and how bonding performance is affected.

Materials used were CFRP plate, epoxy adhesive and steel. The CFRP plate width and thickness were 25 mm and 1.5 mm respectively, with the steel adherend having a larger thickness at 5.5 mm. Two types of adhesives were used, with one (Tc) being described as non-linear, and more ductile than the other (T1), described as linear. The testing was single lap and used a bonding length of 200 mm.

The cyclic temperature testing was carried out in a temperature variation chamber that gave 150, 300 and 500 cycles, with heating and cooling rates of 1.5 °C per minute, cycle times of 3 h and 20 min, and dwelling at the upper and lower temperature limit of 40 °C to −20 °C for 1 h. Subsequent testing of the bond was completed using a single lap shear test at a speed of 0.2 mm·min^{-1}.

When looking at the effect of temperature cycles on CFRP plate properties, there showed little variation in tensile strength, elastic modulus and maximum strain compared to the control; up to 5% variation after 500 cycles. Other similar studies in literature support this [150,151,152]. This suggests that the shear stress that results from a CTE mismatch between carbon fibre and matrix is not enough to limit tensile properties significantly. For the bulk adhesive samples, results also showed that there was not a significant change in tensile strength in the T1 adhesive, but there was a 9% decrease in elastic modulus after 500 cycles. The opposite is found in the Tc adhesive, where after 500 cycles the tensile strength decreased by 17% and yet there was little change in elastic modulus. The reduction in tensile properties was described to be from air voids forming in the adhesive which accumulate fatigue damage around them.

Further analysis looked at the effect that temperature cycles had specifically on the CFRP/steel interface, shown in Table 7. The average ultimate load with the adhesive Tc decreased by 9%. T1 showed little

Table 7
Ultimate load for CFRP/steel joins subject to thermal cycling, .

Specimen	Number of cycles	Average ultimate load (N)
Tc - Control	0	64,500
Tc	150	65,800
Tc	300	58,200
Tc	500	58,600
T1 - Control	0	45,100
T1	150	44,900
T1	300	42,900
T1	500	45,300

adapted from [40]

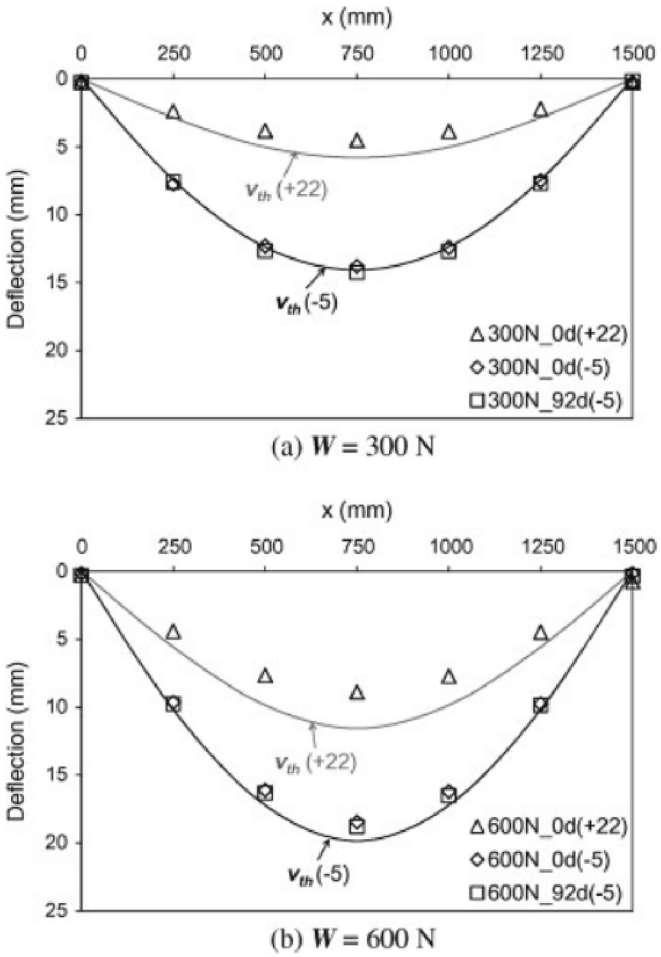

Fig. 33. Deflection profiles for (a) 300 N and (b) 600 N [41].

change and varied less than 5%. Furthermore, the Tc adhesive showed 1.4 times higher ultimate load than T1.

Yoshitake et al [41] looked at the flexural behaviour and hence interfacial bonding integrity of CFRP laminate when bonded to steel and exposed to low temperatures down to −20 °C. The study focuses again on the CTE discrepancy between materials.

The testing involved both a sustained load and H-beam flexural test. Both tests used 2 mm adhesive thickness. The steel strips for the sustained load test were 9 mm in thickness, 125 mm in width and 1600 mm in length. The H-beam had a contact thickness of 8 mm, a width of 100 mm and a length again of 1600 mm. The steel CTE was 12.0 (10^{-6} °C^{-1}) and the CFRP CTE was 0.3 (10^{-6} °C^{-1}).

Firstly, the sustained flexural load test was performed over 100 days, with 3 cycles reaching −5°C to 20 °C, each with an approximate cycle length of 40, 30 and 20 days consecutively. Loads of 300 N and 600 N were applied to the mid-span, with deflections of 4.5 mm and 8.9 mm respectively.

Next, the H-beam test was used to increase the stiffness of the steel to limit the potential for the discrepancy in axial stiffness affecting the bonding behaviour through CFRP and steel debonding. Here, both composite and steel were placed in a freeze–thaw cycle for 336 days under zero external forces and only internal forces due to thermal deformation. Cycles lasted 14 days, and reduced in minimum temperature over time, beginning at −10 °C, dropping to −18 °C, before returning to −10 °C. Flexural testing was undertaken after 0, 28, 84, 168 and 336 days. The control consisted of keeping the H-beams at 20 °C for 336 days. In the testing, a load was monotonically applied at 200 $N{\cdot}s^{-1}$ until debonding/failure occurred.

The results (Fig. 33) from the sustained load test showed that at 300 N and 600 N and −5°C, deflection increased significantly at all points along the span, whilst being independent from sustained load/exposure. The differences were said to be from the CTE mismatch, whilst the similar nature of the curves suggest that the CFRP was firmly bonded throughout.

The results from the H-beam test showed that the ultimate flexural strength with CFRP after low temperature cyclic exposure was equal to the control at room temperature (22 °C), leading to the conclusion that CTE discrepancy effect is negligible under these temperature ranges.

7. Conclusion

This paper has aimed to gather the current research on hybrid composite/metallic driveshafts and covers a wide range of engineering disciplines to assess both their advantages and the challenges they introduce to engineers. Research studies crossing aerospace, automotive, civil and marine engineering have been cited, highlighting the significant advances in understanding FRPs role in these driveshafts. Because of the recent advances in composite technology, a large part of the research has occurred in the last five years alone, and further research into increasing the technologies mechanical, environmental and thermal envelopes must be ongoing for this technology to reach its full potential.

The paper highlights the following:

- The most effective winding layups, fibre orientations and thicknesses for different driveshaft applications.
- The advantages and drawbacks of different coupling methods through changing the composite/metallic interfacial shape.
- The effect of changing the composite, metallic and adhesive material properties effect the overall interfacial integrity.
- That different types of corrosion and liquid absorption can affect the composite/metallic interfacial bond. Also, the usefulness of different testing methods when assessing the post corrosion/immersion of a join.
- The way in which the CTE mismatch between materials can affect the interfacial strength, and the methods in which to test this strength post thermal exposure.

Overall, usage of these driveshafts show wide-ranging usefulness currently, but importantly it is apparent there is huge scope for future application. Developing the research touched upon in this review paper would unlock further uses of these driveshafts, currently impossible with present technology. The future hybrid driveshafts could be more tailored to individual needs; more efficient in transferring torque; less susceptible to wet, corrosive environments and will be able to reach further into the high temperature heart of the gas turbine engine, further increasing the efficiency of flight.

The raw/processed data required to reproduce these findings cannot be shared at this time due to technical or time limitations.

Declaration of Competing Interest

The authors declare that they have no known competing financial interests or personal relationships that could have appeared to influence the work reported in this paper.

Data availability

The data that has been used is confidential.

Acknowledgements

This work was supported through funding from Rolls-Royce plc. The provision of materials and technical support from Rolls-Royce plc is also gratefully acknowledged.

References

[1] Zweben CH. Composites: Overview. Encycl Condens Matter Phys 2005:192–208. https://doi.org/10.1016/B0-12-369401-9/00545-3.
[2] Ashby M. Material property data for engineering materials; 2016. [Online]. Available: http://www.grantadesign.com/download/pdf/booklets/Material_Property_Data_for_Engineering_Materials.pdf.
[3] Tariq M, Nisar S, Shah A, Akbar S, Khan MA, Khan SZ. Effect of hybrid reinforcement on the performance of filament wound hollow shaft. Compos Struct 2018;184:378–87. https://doi.org/10.1016/j.compstruct.2017.09.098.
[4] Ravi A. Design, Comparison and Analysis of a Composite Drive Shaft for an Automobile. Int Rev Appl Eng Res 2014;4(1):21–8.
[5] Nayak SY, Amin NM, Heckadka SS, Vishal SP, Prakash CS, Mabbu R. Design, fabrication and testing of carbon fiber reinforced epoxy drive shaft for all terrain vehicle using filament winding. MATEC Web Conf 2018;153. https://doi.org/10.1051/matecconf/201815304010.
[6] Nadaf AR, Raikar VA. Design & Analysis of Composite Shaft of Passenger Vehicle. Int Res J Eng Technol 2017;4(8):151–8.
[7] Parshuram D, Mangsetty S. Design and Analysis of Composite Hybrid Drive Shaft for Automotives. 2(01) (2013) 160–171.
[8] McElroy MW, Lawrie A, Bond IP. Optimisation of an air film cooled CFRP panel with an embedded vascular network. Int J Heat Mass Transf 2015;88:284–96. https://doi.org/10.1016/j.ijheatmasstransfer.2015.04.071.
[9] Kim SJ, Kim YR, Kim Y, Kim MH, Lee MS. 2D exhaust nozzle with multiple composite layers for IR signature suppression. Results Phys 2020;19. https://doi.org/10.1016/j.rinp.2020.103395.
[10] Poul R, Růžička P, Hanus D, Blahouš K. Design of Carbon Composite Driveshaft for Ultralight Aircraft Propulsion System. Acta Polytech 2006;46(5):40–4.
[11] Özgen GA, Yücetürk K, Tanoğlu M, Aktas E. An Investigation on Hybrid Composite Drive Shaft for Automotive Industry. Int J Mech Mater Eng 2019;13 (4):258–64. https://doi.org/10.5281/zenodo.2643824.
[12] Elanchezhian C, Vijaya Ramnath B, Sripada Raghavendra KN, Muralidharan M, Rekha G. Design and Comparison of the Strength and Efficiency of Drive Shaft made of Steel and Composite Materials. Mater Today Proc 2018;5(1):1000–7. https://doi.org/10.1016/j.matpr.2017.11.176.
[13] Zhao X-L, Bai Y, Al-Mahaidi R, Rizkalla S. Effect of Dynamic Loading and Environmental Conditions on the Bond between CFRP and Steel: State-of-the-Art Review. J Compos Constr 2014;18(3):pp. https://doi.org/10.1061/(asce)cc.1943-5614.0000419.
[14] Tariq M, et al. Effect of carbon fiber winding layer on torsional characteristics of filament wound composite shafts. J Brazilian Soc Mech Sci Eng Apr. 2018;40(4): 198. https://doi.org/10.1007/s40430-018-1099-3.

[15] Sun Z, et al. Vibration characteristics of carbon-fiber reinforced composite drive shafts fabricated using filament winding technology. Compos Struct 2020;241. https://doi.org/10.1016/j.compstruct.2019.111725.

[16] Prasad AS, Ramakrishna S, Madhavi M. Experimental Investigations on Static and Dynamic Parameters of Steel and Composite Propeller Shafts with an Integrated Metallic Joints. Mater Today Proc 2018;5(13):26925–33. https://doi.org/10.1016/j.matpr.2018.08.180.

[17] Sevkat E, Tumer H, Halidun Kelestemur M, Dogan S. Effect of torsional strain-rate and lay-up sequences on the performance of hybrid composite shafts. Mater Des 2014;60:310–9. https://doi.org/10.1016/j.matdes.2014.03.069.

[18] Laberge KE, Handschuh RF, Roberts G, Thorp S. Performance investigation of a full-scale hybrid composite bull gear. Annu Forum Proc - AHS Int 2016;3:2591–7.

[19] LaBerge KE, Johnston JP, Handschuh RF, Roberts GD. Evaluation of a variable thickness hybrid composite bull gear. Annu Forum Proc - AHS Int 2018;2018May.

[20] Gauntt SM, Campbell RL. Characterization of a hybrid (Steel-composite) gear with various composite materials and layups. AIAA Scitech 2019 Forum 2019. https://doi.org/10.2514/6.2019-0146.

[21] Waller MD, McIntyre SM, Koudela KL. Composite Materials for Hybrid Aerospace Gears. J Am Helicopter Soc 2020;65(4):1–11. https://doi.org/10.4050/jahs.65.042010.

[22] Kim WT, Lee DG. Torque transmission capabilities of adhesively bonded tubular lap joints for composite drive shafts. Compos Struct 1995;30(2):229–40. https://doi.org/10.1016/0263-8223(95)80017-4.

[23] Lee DG, Kim HS, Kim JW, Kim JK. Design and manufacture of an automotive hybrid aluminum/composite drive shaft. Compos Struct 2004;63(1):87–99. https://doi.org/10.1016/S0263-8223(03)00136-3.

[24] Choi JK, Lee DG. Experimental investigation of the static torque transmission capabilities of the adhesively bonded single lap joints. J Mater Process Tech 1995;48(1–4):341–7. https://doi.org/10.1016/0924-0136(94)01667-P.

[25] Henry TC, Bakis CE, Miller SW, Smith EC. Multi-objective optimal design of composite rotorcraft driveshaft including strain rate and temperature effects. Compos Struct 2015;128:42–53. https://doi.org/10.1016/j.compstruct.2015.03.029.

[26] Henry TC, Riddick JC, Mills BT, Habtour EM. Composite driveshaft prototype design and survivability testing. J Compos Mater 2017;51(16):2377–86. https://doi.org/10.1177/0021998316670478.

[27] Kim JK, Lee DG, Cho DH. Investigation of Adhesively Bonded Joints for Composite Propeller Shafts. J Compos Mater 2001;35(11):999–1021. https://doi.org/10.1106/j5qd-b843-qexc-18eb.

[28] Alves DL, Campilho RDSG, Moreira RDF, Silva FJG, Cardoso MG. Effect of material hybridization on the strength of scarf adhesive joints. Procedia Manuf 2019;38:1244–51. https://doi.org/10.1016/j.promfg.2020.01.216.

[29] Carbas RJC, Palmares MP, Da Silva LFM. Experimental and FE study of hybrid laminates aluminium carbon-fibre joints with different lay-up configurations. Manuf Rev 2020;7. https://doi.org/10.1051/mfreview/2019027.

[30] Jimenez-Vicaria JD, Pulido MDG, Castro-Fresno D. Influence of carbon fibre stiffness and adhesive ductility on CFRP-steel adhesive joints with short bond lengths. Constr Build Mater 2020;260. https://doi.org/10.1016/j.conbuildmat.2020.119758.

[31] Amraei M, Zhao XL, Björk T, Heidarpour A. Bond characteristics between high/ultra-high strength steel and ultra-high modulus CFRP laminates. Eng Struct 2020;205. https://doi.org/10.1016/j.engstruct.2019.110094.

[32] Al-Mosawe A, Al-Mahaidi R, Zhao XL. Bond behaviour between CFRP laminates and steel members under different loading rates. *FRPRCS-12/APFIS-2015 - Jt. Conf. 12th Int. Symp. Fiber Reinf. Polym. Reinf. Concr. Struct. FRPRCS 2015 5th Asia-Pacific Conf. Fiber Reinf. Polym. Struct. APFIS 2015*; 2015.

[33] Al-Shawaf A, Al-Mahaidi R, Zhao XL. Study on bond characteristics of CFRP/steel double-lap shear joints at subzero temperature exposure. Compos Civ Eng CICE 2020;2006:71–4.

[34] Al-Shawaf A, Zhao XL. Adhesive rheology impact on wet lay-up CFRP/steel joints' behaviour under infrastructural subzero exposures. Compos Part B Eng 2013;47:207–19. https://doi.org/10.1016/j.compositesb.2012.11.012.

[35] Nguyen TC, Bai Y, Zhao XL, Al-Mahaidi R. Mechanical characterization of steel/CFRP double strap joints at elevated temperatures. Compos Struct 2011;93(6):1604–12. https://doi.org/10.1016/j.compstruct.2011.01.010.

[36] Liu HB, Zhao XL, Bai Y, Raman RKS, Rizkalla S, Bandyopadhyay S. The Effect of Elevated Temperature on the Bond between High Modulus CFRP Sheet and Steel. Aust J Struct Eng 2014;15(4):355–66.

[37] Xu S, Li H, Wang Y, Wang Y, Wang Y. Influence of corrosion on the bond behavior in CFRP-steel single lap joints. Constr Build Mater 2020;236. https://doi.org/10.1016/j.conbuildmat.2019.117607.

[38] Ocaña R, Arenas JM, Alía C, Narbón JJ. Evaluation of Degradation of Structural Adhesive Joints in Functional Automotive Applications. Procedia Eng 2015;132:716–23. https://doi.org/10.1016/j.proeng.2015.12.552.

[39] Oudad W, et al. Effect of humidity absorption by the adhesive on the performances of bonded composite repairs in aircraft structures. Compos Part B Eng 2012;43(8):3419–24. https://doi.org/10.1016/j.compositesb.2012.01.028.

[40] Wang Z, Xian G. Effects of thermal expansion coefficients discrepancy on the CFRP and steel bonding. Constr Build Mater 2021;269. https://doi.org/10.1016/j.conbuildmat.2020.121356.

[41] Yoshitake I, Tsuda H, Itose J, Hisabe N. Effect of discrepancy in thermal expansion coefficients of CFRP and steel under cold temperature. Constr Build Mater 2014;59:17–24. https://doi.org/10.1016/j.conbuildmat.2014.02.051.

[42] Lee LJ. Modeling and Computer Simulation of Reactive Processing. Compr Polym Sci Suppl 1989:575–617. https://doi.org/10.1016/b978-0-08-096701-1.00238-x.

[43] Sorrentino L, et al. Robotic filament winding: An innovative technology to manufacture complex shape structural parts. Compos Struct 2019;220:699–707. https://doi.org/10.1016/j.compstruct.2019.04.055.

[44] Capela C, Ferreira JAM, Febra T, Costa JD. Fatigue strength of tubular carbon fibre composites under bending/torsion loading. Int J Fatigue 2015;70:216–22. https://doi.org/10.1016/j.ijfatigue.2014.09.008.

[45] Pater Z, Gontarz A, Tomczak J, Bulzak T. Producing hollow drive shafts by rotary compression. Arch Civ Mech Eng 2015;15(4):917–24. https://doi.org/10.1016/j.acme.2014.10.002.

[46] Fragoudakis R. Strengths and Limitations of Traditional Theoretical Approaches to FRP Laminate Design against Failure. Eng Fail Anal 2020. https://doi.org/10.5772/intechopen.89729.

[47] Reddy PSK, Krishna TH, Optimum Design And Analysis Of Filament Wound Composite Tubes In Pure And Combined Loading 1(8) (2012) 1–4.

[48] Biron M, *Thermoplastics and Thermoplastic Composites: Second Edition,* 2012. 10.1016/C2011-0-05605-3.

[49] Rosato DV, Rosato DV. Plastics Engineered Product Design. Plast Eng Prod Des 2003:1–568. https://doi.org/10.1016/B978-1-85617-416-9.X5000-5.

[50] Quanjin M, Rejab MRM, Idris MS, Bachtiar B, Siregar JP, Harith MN. Design and optimize of 3-axis filament winding machine. *IOP Conf Ser* Mater Sci Eng 2017;257(1):pp. https://doi.org/10.1088/1757-899X/257/1/012039.

[51] Rejab MRM, Noor MM. Modification and Testing of Four Axes Filament Winding Machine. Design 2008:1505–9.

[52] Hearn EJ. Mechanics of Materials 1. In: *Structural and Stress Analysis*. 3rd edition2. Butterworth Heinemann; 1997. p. 481.

[53] Puck A, Schürmann H. Failure analysis of FRP laminates by means of physically based phenomenological models. Fail Criteria Fibre-Reinforced-Polymer Compos 2004:832–76. https://doi.org/10.1016/B978-008044475-8/50028-7.

[54] Montagnier O, Hochard C. Optimisation of hybrid high-modulus/high-strength carbon fibre reinforced plastic composite drive shafts. Mater Des 2013;46:88–100. https://doi.org/10.1016/j.matdes.2012.09.035.

[55] Sharan Gupta U, et al. Study on the effects of fiber orientation on the mechanical properties of natural fiber reinforced epoxy composite by finite element method. Mater Today Proc 2021;45:7885–93. https://doi.org/10.1016/j.matpr.2020.12.614.

[56] Khalkhali A, Nikghalb E, Norouzian M. Multi-objective optimization of hybrid carbon/glass fiber reinforced epoxy composite automotive drive shaft. Int J Eng Trans A Basics 2015;28(4):600–9. https://doi.org/10.5829/idosi.ije.2015.28.04a.12.

[57] Abu Talib AR, Ali A, Badie MA, Azida Che Lah N, Golestaneh AF. Developing a hybrid, carbon/glass fiber-reinforced, epoxy composite automotive drive shaft. Mater Des 2010;31(1):514–21. https://doi.org/10.1016/j.matdes.2009.06.015.

[58] Vidya Sagar SB. Investigation of the Effect of Fiber Orientation on FML Hollow Shaft Subjected to Static Torsion Loading. *J Theor Comput Sci* 2015;02(02). 10.4172/jtco.1000126.

[59] Cherniaev A, Komarov V. Multistep Optimization of Composite Drive Shaft Subject to Strength, Buckling, Vibration and Manufacturing Constraints. Appl Compos Mater 2015;22(5):475–87. https://doi.org/10.1007/s10443-014-9418-z.

[60] Badie MA, Mahdi A, Abutalib AR, Abdullah EJ, Yonus R. Automotive Composite Driveshafts : Investigation of the Design. Int J Eng Technol 2006;3(2):227–37.

[61] Shokrieh MM, Hasani A, Lessard LB. Shear buckling of a composite drive shaft under torsion. Compos Struct 2004;64(1):63–9. https://doi.org/10.1016/S0263-8223(03)00214-9.

[62] Bert CW, Do Kim C. Analysis of buckling of hollow laminated composite drive shafts. Compos Sci Technol 1995;53(3):343–51. https://doi.org/10.1016/0266-3538(95)00006-2.

[63] Badie MA, Mahdi E, Hamouda AMS. An investigation into hybrid carbon/glass fiber reinforced epoxy composite automotive drive shaft. Mater Des 2011;32(3):1485–500. https://doi.org/10.1016/j.matdes.2010.08.042.

[64] Laux T, Gan KW, Dulieu-Barton JM, Thomsen OT. Ply thickness and fibre orientation effects in multidirectional composite laminates subjected to combined tension/compression and shear. Compos Part A Appl Sci Manuf 2020;133. https://doi.org/10.1016/j.compositesa.2020.105864.

[65] Amacher R, Cugnoni J, Botsis J, Sorensen L, Smith W, Dransfeld C. Thin ply composites: Experimental characterization and modeling of size-effects. Compos Sci Technol 2014;101:121–32. https://doi.org/10.1016/j.compscitech.2014.06.027.

[66] Minus ML, Kumar S. The processing, properties, and structure of carbon fibers. JOM 2005;57(2):52–8. https://doi.org/10.1007/s11837-005-0217-8.

[67] Crandall SH, Dahl NC, Dill EH. *An Introduction to the Mechanics of Solids* 1960:13(8). 10.1063/1.3057081.

[68] Sathishkumar TP, Satheeshkumar S, Naveen J. Glass fiber-reinforced polymer composites - A review. J Reinf Plast Compos 2014;33(13):1258–75. https://doi.org/10.1177/0731684414530790.

[69] Rajmane PSM, Chopade MA. Investigation of Effect of Stacking Sequence and Fibre Orientation on Maximum Torque Transmission Capacity of an Composite Automobile Driveshaft by Analytical & FEA 2014;3(11):31–37.

[70] Naik NK, Asmelash A, Kavala VR, Ch V. Interlaminar shear properties of polymer matrix composites: Strain rate effect. Mech Mater 2007;39(12):1043–52. https://doi.org/10.1016/j.mechmat.2007.05.003.

[71] Yu X, Chen L, Fang Q, Jiang X, Zhou Y. A review of the torsional split hopkinson bar. Adv Civ Eng 2018;2018. https://doi.org/10.1155/2018/2719741.

[72] Ma J, Wei Q, Fan H, Qi Z, Hu N. Mechanical Properties Evolution and Damage Mechanism of Kevlar Fiber under Ozone Exposure in Near-Space Simulation. Coatings 2022;12(5):pp. https://doi.org/10.3390/coatings12050584.

[73] Broughton WR, Maxwell AS. Accelerated environmental ageing of polymeric materials; 2007.
[74] Behera A, Behera RK, Sahu P, Swain RR, Mahapatra TR. Tensile and Failure Behavior of Kevlar Fiber Reinforced Epoxy Matrix Composite Exposed to Different Environmental Conditions. Mater Today Proc 2018;5(9):20250–6. https://doi.org/10.1016/j.matpr.2018.06.396.
[75] Reis PNB, Silva MP, Santos P, Parente J, Valvez S. Effect of hostile solutions on the residual fatigue life of kevlar/epoxy composites after impact loading. Molecules 2021;26(18):pp. https://doi.org/10.3390/molecules26185520.
[76] Silva MP, Santos P, Parente JM, Valvez S, Reis PNB. Effect of different hostile solutions on mechanical properties of composite materials. Procedia Struct Integr 2022;vol. 37, no. C:841–6. https://doi.org/10.1016/j.prostr.2022.02.017.
[77] Agarwal G, Johri N. Experimental investigations on mechanical properties and abrasive wear response of glass, kevlar and carbon fabric reinforced composites. Mater Today Proc 2021;46:7966–72. https://doi.org/10.1016/j.matpr.2021.02.704.
[78] Joselin R, Wilson WJ. Investigation on impact strength properties of kevlar fabric using different shear thickening fluid composition. *Def Sci J* 2014;64(3):236–43. 10.14429/dsj.64.7322.
[79] Mayrides B, Smith EC, Wang KW. Analysis and synthesis of highly flexible helicopter drivelines with flexible matrix composite shafting. Annu Forum Proc - AHS Int 2005;2:1582–95.
[80] Minak G, Abrate S, Ghelli D, Panciroli R, Zucchelli A. Residual torsional strength after impact of CFRP tubes. Compos Part B Eng 2010;41(8):637–45. https://doi.org/10.1016/j.compositesb.2010.09.021.
[81] Ochoa OO, Roschke P, Bafrali R. Damage tolerance of composite tubes under compressive loading. Compos Struct 1991;19(1):1–14. https://doi.org/10.1016/0263-8223(91)90072-7.
[82] Karthikeyan P, Gobinath R, Ajith Kumar L, Xavier Jenish D. Design and Analysis of Drive Shaft using Kevlar/Epoxy and Glass/Epoxy as a Composite Material. IOP Conf Ser Mater Sci Eng 2017;197(1). https://doi.org/10.1088/1757-899X/197/1/012048.
[83] Rangaswamy T, Vijayarangan S. Optimal sizing and stacking sequence of composite drive shafts. Mater Sci 2005;11(2):133–9.
[84] Jambor E. Manufacturing and testing of spline geometry using carbon fiber reinforced composite; 2016.
[85] RollsRoyce Plc. *The Jet Engine*. 1996.
[86] Darmstadt PR, Robuck M. Composites for advanced drive systems, a systems analysis - Revolutionary vertical lift technology (RVLT). *Annu Forum Proc - AHS Int* 2018;2018-May.
[87] Mohd Tobi AL, Ismail AE. Development in Geared Turbofan Aeroengine. IOP Conf Ser Mater Sci Eng 2016;131(1):pp. https://doi.org/10.1088/1757-899X/131/1/012019.
[88] Dewhirst M. Transmission shaft joint design. US7874925B2, 2011.
[89] Kim HS, Lee DG. Optimal design of the press fit joint for a hybrid aluminum/composite drive shaft. Compos Struct 2005;70(1):33–47. https://doi.org/10.1016/j.compstruct.2004.08.010.
[90] Oessenich R, Freund A, Filler M, Renner O, Pabst A. Shaft of a gas-turbine engine, in particulara radal shaft ora shaftarrangedatan angle to the machine axis. US 9,217,463 B2; 2015.
[91] Wang HT, Liu SS, Liu QL, Pang YY, Shi JW. Influences of the joint and epoxy adhesive type on the CFRP-steel interfacial behavior. J Build Eng 2021;43. https://doi.org/10.1016/j.jobe.2021.103167.
[92] Parashar A, Mertiny P. Adhesively bonded composite tubular joints: Review. Int J Adhes Adhes 2012;38:58–68. https://doi.org/10.1016/j.ijadhadh.2012.05.004.
[93] Handschuh RF, Stringer DB, Dykas BD, Kohlman LW. Hybrid Gear Preliminary Results—Application of Composites to Dynamic Mechanical Components. American Helicopter Society; 2012.
[94] Marsh G. Automating aerospace composites production with fibre placement. Reinf Plast 2011;55(3):32–7. https://doi.org/10.1016/S0034-3617(11)70075-3.
[95] Catera PG, Gagliardi F, Mundo D, De Napoli L, Matveeva A, Farkas L. Multi-scale modeling of triaxial braided composites for FE-based modal analysis of hybrid metal-composite gears. Compos Struct 2017;182:116–23. https://doi.org/10.1016/j.compstruct.2017.09.017.
[96] Moreira RDF, Campilho RDSG. Strength improvement of adhesively-bonded scarf repairs in aluminium structures with external reinforcements. Eng Struct 2015;101:99–110. https://doi.org/10.1016/j.engstruct.2015.07.001.
[97] Juuma T. Torsional fretting fatigue strength of a shrink-fitted shaft with a grooved hub. Tribol Int 2000;33(8):537–43. https://doi.org/10.1016/S0301-679X(00)00102-X.
[98] El Zoghby A, et al. Torsional Buckling Optimization of Composite Drive Shafts. World Appl Sci J 2016;33(3):517–24.
[99] Patnaik S, Hopkins D. *Strength of Materials A New Unified Theory for the 21st Century*; 2004.
[100] Duncan B. Developments in testing adhesive joints. In: *Advances in Structural Adhesive Bonding*; 2010. p. 389–436. 10.1533/9781845698058.3.389.
[101] Kwon YW. Design and analysis of bonded joints and repair. Compr Compos Mater II 2018;8–8:157–77. https://doi.org/10.1016/B978-0-12-803581-8.09976-8.
[102] Ben Ouezdou M, Bae S, Belarbi A. Effective bond length of externally bonded FRP sheets. In: *Proceedings of the 4th International Conference on FRP Composites in Civil Engineering, CICE 2008*; 2008.
[103] Teng JG, Yu T, Fernando D. Strengthening of steel structures with fiber-reinforced polymer composites. J Constr Steel Res 2012;78:131–43. https://doi.org/10.1016/j.jcsr.2012.06.011.
[104] Fawzia S, Al-Mahaidi R, Zhao XL, Rizkalla S. Strengthening of circular hollow steel tubular sections using high modulus CFRP sheets. Constr Build Mater 2007;21(4):839–45. https://doi.org/10.1016/j.conbuildmat.2006.06.014.
[105] Xia SH, Teng JG. Behaviour of FRP-to-steel bonded joints. *Proc Int Symp Bond Behav FRP Struct BBFS 2005*; 2005. p. 411–8.
[106] Yu T, Fernando D, Teng JG, Zhao XL. Experimental study on CFRP-to-steel bonded interfaces. Compos Part B Eng 2012;43(5):2279–89. https://doi.org/10.1016/j.compositesb.2012.01.024.
[107] Nozaka K, Shield Carol K, Hajjar Jerome F. Effective Bond Length of Carbon-Fiber-Reinforced Polymer Strips Bonded to Fatigued Steel Bridge I-Girders. J Bridg Eng 2005;10(2):195–205.
[108] Duncan B, Broughton B. Characterising strength of adhesion. Meas Good Pract Guid 2004;72:54–5.
[109] Alderliesten R. On the Development of Hybrid Material Concepts for Aircraft Structures. Recent Patents Eng 2009;3(1):25–38. https://doi.org/10.2174/187221209787259893.
[110] AirBus. A380, world's largest commercial aircraft, successfully takes to the skies; 2005. http://www.airbus.com.
[111] Bellini C, Di Cocco V, Iacoviello F, Sorrentino L. Comparison between long and short beam flexure of a carbon fibre based FML. Procedia Struct Integr 2020;26:120–8. https://doi.org/10.1016/j.prostr.2020.06.015.
[112] Simões BD, Nunes PDP, Ramezani F, Carbas RJC, Marques EAS, da Silva LFM. Experimental and Numerical Study of Thermal Residual Stresses on Multimaterial Adherends in Single-Lap Joints. Materials (Basel) 2022;15(23):pp. https://doi.org/10.3390/ma15238541.
[113] Fawzia S. Evaluation of shear stress and slip relationship of composite lap joints. Compos Struct 2013;100:548–53. https://doi.org/10.1016/j.compstruct.2012.12.027.
[114] Lisle T, Little C, Aylott C. Bending fatigue strength of aerospace quality gear steels at ambient and elevated temperatures. Int J Fatigue 2022;164. https://doi.org/10.1016/j.ijfatigue.2022.107125.
[115] Jiao H, Zhao XL. CFRP strengthened butt-welded very high strength (VHS) circular steel tubes. Thin-Walled Struct 2004;42(7):963–78. https://doi.org/10.1016/j.tws.2004.03.003.
[116] Al-Mosawe A, Al-Mahaidi R, Zhao X-L. Experimental and Numerical Study on Strengthening of Steel Members Subjected to Impact Loading Using Ultrahigh Modulus CFRP. J Compos Constr 2016;20(6):pp. https://doi.org/10.1061/(asce)cc.1943-5614.0000703.
[117] Sauder C, Lamon J, Pailler R. The tensile behavior of carbon fibers at high temperatures up to 2400°C. Carbon N Y 2004;42(4):715–25. https://doi.org/10.1016/j.carbon.2003.11.020.
[118] Uthaman A, Xian G, Thomas S, Wang Y, Zheng Q, Liu X. Durability of an epoxy resin and its carbon fiber-reinforced polymer composite upon immersion in water, acidic, and alkaline solutions. Polymers (Basel) 2020;12(3):pp. https://doi.org/10.3390/polym12030614.
[119] Corveleyn S, Lachaud F, Berthet F, Rossignol C. Long-term creep behavior of a short carbon fiber-reinforced PEEK at high temperature: Experimental and modeling approach. Compos Struct 2022;290. https://doi.org/10.1016/j.compstruct.2022.115485.
[120] Yang H, Liu J, Ji M, Yang S. Novel Thermoplastic Polyimide Composite Materials. Thermoplast - Compos Mater 2012. https://doi.org/10.5772/34945.
[121] Gabrion X, Placet V, Trivaudey F, Boubakar L. About the thermomechanical behaviour of a carbon fibre reinforced high-temperature thermoplastic composite. Compos Part B Eng 2016;95:386–94. https://doi.org/10.1016/j.compositesb.2016.03.068.
[122] Al-Shawaf A, Al-Mahaidi R, Zhao XL. Effect of elevated temperature on bond behaviour of high modulus CFRP/steel double-strap joints. Aust J Struct Eng 2009;10(1):63–74. https://doi.org/10.1080/13287982.2009.11465033.
[123] Alam P, Mamalis D, Robert C, Floreani C, Brádaigh CMÓ. The fatigue of carbon fibre reinforced plastics - A review. Compos Part B Eng 2019;166:555–79. https://doi.org/10.1016/j.compositesb.2019.02.016.
[124] Varna J, Joffe R, Berglund LA, Lundström TS. Effect of voids on failure mechanisms in RTM laminates. Compos Sci Technol 1995;53(2):241–9. https://doi.org/10.1016/0266-3538(95)00024-0.
[125] Fiedler B, Schulte K. Reliability and life prediction of composite structures. Compos Sci Technol 2006;66(5):615. https://doi.org/10.1016/j.compscitech.2005.08.013.
[126] Guo ZS, Liu L, Zhang BM, Du S. Critical void content for thermoset composite laminates. J Compos Mater 2009;43(17):1775–90. https://doi.org/10.1177/0021998306065289.
[127] Zhu H, Wu B, Li D, Zhang D, Chen Y. Influence of Voids on the Tensile Performance of Carbon/epoxy Fabric Laminates. J Mater Sci Technol 2011;27(1):69–73. https://doi.org/10.1016/S1005-0302(11)60028-5.
[128] Korkees F, Arnold C, Alston S. An investigation of the long-term water uptake behavior and mechanisms of carbon fiber/977-2 epoxy composites. Polym Eng Sci 2018;58(12):2175–84. https://doi.org/10.1002/pen.24830.
[129] Arnold JC, Alston S, Korkees F, Dauhoo S, Adams R, Older R. Design Optimisation of Carbon Fibre Epoxy Composites Operating in Humid Atmospheres. In: *Composites UK 10th Annual Conference: Innovation in Composites*; 2010.
[130] Korkees F, Arnold C, Alston S. Water absorption and low-energy impact and their role in the failure of ±45° carbon fibre composites. Polym Compos 2018;39(8):2771–82. https://doi.org/10.1002/pc.24269.
[131] Korkees F, Alston S, Arnold C. Directional diffusion of moisture into unidirectional carbon fiber/epoxy Composites: Experiments and modeling. Polym Compos 2018;39:E2305–15. https://doi.org/10.1002/pc.24626.

[132] Jarrett W, Korkees F. Environmental impact investigation on the interlaminar properties of carbon fibre composites modified with graphene nanoparticles. Polymer (Guildf) Jun. 2022;252:124921. https://doi.org/10.1016/j.polymer.2022.124921.
[133] Capiel G, Uicich J, Fasce D, Montemartini PE. Diffusion and hydrolysis effects during water aging on an epoxy-anhydride system. Polym Degrad Stab 2018;153:165–71. https://doi.org/10.1016/j.polymdegradstab.2018.04.030.
[134] Chateauminois A, Chabert B, Soulier JP, Vincent L. Dynamic mechanical analysis of epoxy composites plasticized by water: Artifact and reality. Polym Compos 1995;16(4):288–96. https://doi.org/10.1002/pc.750160405.
[135] Borrie D, Al-saadi S, Zhao XL, Singh Raman RK, Bai Y. Bonded cfrp/steel systems, remedies of bond degradation and behaviour of CFRP repaired steel: An overview. Polymers (Basel) 2021;13(9):pp. https://doi.org/10.3390/polym13091533.
[136] Song G-L, Zhang C, Chen X, Zheng D. Galvanic activity of carbon fiber reinforced polymers and electrochemical behavior of carbon fiber. Corros Commun 2021;1:26–39. https://doi.org/10.1016/j.corcom.2021.05.003.
[137] Lu F, Zhang X, Tang Z, Liu M. Galvanic corrosion behavior between carbon fiber reinforced plastic materials and aluminum alloys. J Chinese Soc Corros Prot 2005;25(1):39–43.
[138] Wu X, Sun J, Wang J, Jiang Y, Li J. Investigation on galvanic corrosion behaviors of CFRPs and aluminum alloys systems for automotive applications. Mater Corros 2019;70(6):1036–43. https://doi.org/10.1002/maco.201810635.
[139] Torres-Acosta AA. Galvanic Corrosion of Steel in Contact with Carbon-Polymer Composites. II: Experiments in Concrete. J Compos Constr 2002;6(2):116–22. https://doi.org/10.1061/(asce)1090-0268(2002)6:2(116).
[140] De Meyere RMG, et al. A novel trench fibre push-out method to evaluate interfacial failure in long fibre composites. J Mater Res 2021;36(11):2305–14. https://doi.org/10.1557/s43578-021-00153-1.
[141] Jurkiewiez B, Tout F, Ferrier E. Push-out and bending tests of steel-concrete adhesively bonded composite elements. Eng Struct 2021;231. https://doi.org/10.1016/j.engstruct.2020.111717.
[142] Wang D, Han L, Kang M, Wan M, Ju Y. Influence of corrosion on the bond performance of reinforcements and basalt fibre high strength concrete. Case Stud Constr Mater 2022;17. https://doi.org/10.1016/j.cscm.2022.e01394.
[143] Robuschi S, Tengattini A, Dijkstra J, Fernandez I, Lundgren K. A closer look at corrosion of steel reinforcement bars in concrete using 3D neutron and X-ray computed tomography. Cem Concr Res 2021;144. https://doi.org/10.1016/j.cemconres.2021.106439.
[144] Fernandez I, Berrocal CG. Mechanical Properties of 30 Year-Old Naturally Corroded Steel Reinforcing Bars. Int J Concr Struct Mater 2019;13(1):pp. https://doi.org/10.1186/s40069-018-0308-x.
[145] François R, Khan I, Dang VH. Impact of corrosion on mechanical properties of steel embedded in 27-year-old corroded reinforced concrete beams. Mater Struct Constr 2013;46(6):899–910. https://doi.org/10.1617/s11527-012-9941-z.
[146] Teng JG, Fernando D, Yu T, Zhao XL. Treatment of steel surfaces for effective adhesive bonding. *Adv FRP Compos Civ Eng - Proc 5th Int Conf FRP Compos Civ Eng CICE 2010*; 2011. p. 865–868, 10.1007/978-3-642-17487-2_190.
[147] Broughton W. Testing the Mechanical, Thermal and Chemical Properties of Adhesives for Marine Environments. In: *Adhesives in Marine Engineering*; 2012. p. 99–154. 10.1016/B978-1-84569-452-4.50006-0.
[148] Byerly DV. The use of continuous fiber composites in driveshafts. SAE Tech Pap 1996. https://doi.org/10.4271/962208.
[149] Dong C, Li K, Jiang Y, Arola D, Zhang D. Evaluation of thermal expansion coefficient of carbon fiber reinforced composites using electronic speckle interferometry. Opt Express 2018;26(1):531. https://doi.org/10.1364/oe.26.000531.
[150] Pang YY, Wu G, Wang HT, Su ZL, He XY. Experimental study on the bond behavior of the CFRP-steel interface under the freeze–thaw cycles. J Compos Mater 2020;54(1):13–29. https://doi.org/10.1177/0021998319851191.
[151] Nardone F, Di Ludovico M, De Caso FJ, Basalo Y, Prota A, Nanni A. Tensile behavior of epoxy based FRP composites under extreme service conditions. Compos Part B Eng 2012;43(3):1468–74. https://doi.org/10.1016/j.compositesb.2011.08.042.
[152] Pang Y, Wu G, Wang H, Liu Y. Interfacial bond-slip degradation relationship between CFRP plate and steel plate under freeze-thaw cycles. Constr Build Mater 2019;214:242–53. https://doi.org/10.1016/j.conbuildmat.2019.04.114.